

Disorders of the Nervous System

# Cell-Type Specific Channelopathies in the Prefrontal Cortex of the *fmr1*-/- Mouse Model of Fragile X Syndrome<sup>1,2,3</sup>

Brian E. Kalmbach,  Daniel Johnston, and Darrin H. BragerDOI: <http://dx.doi.org/10.1523/ENEURO.0114-15.2015>

Center for Learning and Memory, The University of Texas at Austin, C7000, Austin, Texas 78712

## Abstract

Fragile X syndrome (FXS) is caused by transcriptional silencing of the *fmr1* gene resulting in the loss of fragile X mental retardation protein (FMRP) expression. FXS patients display several behavioral phenotypes associated with prefrontal cortex (PFC) dysfunction. Voltage-gated ion channels, some of which are regulated by FMRP, heavily influence PFC neuron function. Although there is evidence for brain region-specific alterations to the function a single type of ion channel in FXS, it is unclear whether subtypes of principal neurons within a brain region are affected uniformly. We tested for alterations to ion channels critical in regulating neural excitability in two subtypes of prefrontal L5 pyramidal neurons. Using somatic and dendritic patch-clamp recordings, we provide evidence that the functional expression of h-channels ( $I_h$ ) is down-regulated, whereas A-type  $K^+$  channel function is up-regulated in pyramidal tract-projecting (PT) neurons in the *fmr1*-/- mouse PFC. This is the opposite pattern of results from published findings from hippocampus where  $I_h$  is up-regulated and A-type  $K^+$  channel function is down-regulated. Additionally, we find that somatic Kv1-mediated current is down-regulated, resulting in increased excitability of *fmr1*-/- PT neurons. Importantly, these h- and  $K^+$  channel differences do not extend to neighboring intratelencephalic-projecting neurons. Thus, the absence of FMRP has divergent effects on the function of individual types of ion channels not only between brain regions, but also variable effects across cell types within the same brain region. Given the importance of ion channels in regulating neural circuits, these results suggest cell-type-specific phenotypes for the disease.

**Key words:** dendrite; excitability; fragile X syndrome; ion channel; prefrontal cortex

## Significance Statement

Voltage-gated ion channels regulate the excitability of neurons and are altered in fragile X syndrome (FXS), the most common form of inherited mental retardation. In the *fmr1*-/- mouse model of FXS, we found neuron-type-specific alterations in the function of a group of ion channels within the prefrontal cortex, a brain region associated with many cognitive deficits in FXS. Because of these alterations, neurons with subcortical projections display enhanced excitability while those without subcortical projections do not. This finding highlights the need to understand FXS and tailor its treatment in a cell-type-specific manner.

## Introduction

Fragile X syndrome (FXS) is the most common form of inherited mental retardation and the leading identified

D.H.B. performed the research; B.E.K. and D.H.B. analyzed data; B.K., D.J., and D.H.B. wrote the paper.

<sup>3</sup>This work was supported by National Institutes of Health Grants R01 MH094839 (D.J.), R01 MH100510 (D.H.B.), F32 MH090694 (B.E.K.), and a FRAXA research grant (D.H.B.). We thank Komal Parikh and William Taylor for their assistance with surgery, and R. Chitwood and N. Desai for their thoughtful comments on earlier versions of this paper.

Received September 24, 2015; accepted October 28, 2015; First published November 04, 2015.

<sup>1</sup>The authors report no conflict of interest.

<sup>2</sup>Contributions: B.E.K., D.J., and D.H.B. designed the research; B.E.K. and

monogenic cause of autism. Fragile X mental retardation protein (FMRP), the protein absent in FXS, regulates neuron function via multiple mechanisms, including protein-protein interactions, translational control, and protein trafficking (Hagerman et al., 2005; Bhakar et al., 2012; Santoro et al., 2012; Brager and Johnston, 2014). FMRP is capable of binding to mRNA for several ion channels and is known to interact with ion channel-associated proteins (Brown et al., 2010; Darnell et al., 2011; Brager and Johnston, 2014). Although there is evidence for brain region-specific alterations to channel function in FXS, (for review, see Contractor et al., 2015), it is unclear whether these effects are uniform across neuron types within a brain region. Here, we provide evidence for neuron-type-specific alterations to ion channel function within the prefrontal cortex (PFC) of *fmr1*-/*y* mouse.

Neuronal dysfunction in the *fmr1*-/*y* mouse can be attributed to differences in several types of ion channels (Meredith et al., 2007; Strumbos et al., 2010; Brager et al., 2012; Deng et al., 2013; Routh et al., 2013; Zhang et al., 2014). In some cases, reports are conflicting as to the effect of the loss of FMRP on a given type of ion channel. Some have reported an increase (Lee et al., 2011) in Kv4/A-type K<sup>+</sup> channel expression, whereas others have found a decrease (Gross et al., 2011; Routh et al., 2013). Similarly, h-channels have been reported to be up-regulated in hippocampus (Brager et al., 2012), but down-regulated in L5B neurons of somatosensory cortex (Zhang et al., 2014).

We tested the hypothesis that the absence of FMRP has different effects on the function of a single type of ion channel in PFC, a brain region containing a heterogeneous neuron population and that is implicated in behavioral deficits associated with FXS (Menon et al., 2004; Krueger et al., 2011; Wang et al., 2012; Dembrow and Johnston, 2014). Using current-clamp and outside-out patch-clamp recordings from *fmr1*-/*y* mice we provide evidence that  $I_h$  (the current mediated by h-channels) is down-regulated in pyramidal tract (PT)-projecting neurons. This is in contrast to hippocampal CA1 pyramidal neurons, but similar to L5 neurons in somatosensory cortex. Using outside-out patch-clamp recordings, we measured three distinct types of potassium currents: rapidly inactivating A-type current, mediated by putative Kv4 channels; a slowly inactivating current, mediated by putative Kv1 channels; and a sustained current. Again, in contrast to hippocampus, we find that the maximum putative Kv4-mediated current is increased in PT neurons. Additionally, the maximum putative Kv1-mediated current is decreased at the soma of PT neurons, resulting in increased excitability. Notably, these somatic K<sup>+</sup> channel differences do not extend to neighboring intra-

telencephalic-projecting (IT) neurons within L5. Thus, the absence of FMRP has divergent effects on a given type of ion channel in different cell types, even within a single brain region. These findings highlight the need to understand FXS and its treatment in a neuron type/brain region-specific manner.

## Materials and Methods

### Bead infusions

All procedures involving animals were approved by the Institutional Animal Care and Use Committee. Male wild-type (WT; C57BL/6) and *fmr1*-/*y* mice were anesthetized with isoflurane (1–4% mixed in oxygen) and prepared for stereotaxic injection of retrograde transported fluorescent-labeled microspheres (Lumafuor). Beads (100 nl) were injected into the pons (in millimeters relative to bregma: posterior 4.2; lateral 0.4; ventral 4.5), mPFC (anterior 1.0–1.5; lateral 0.45; ventral 1–2), or striatum (posterior 0.4–1.0; lateral 2.25; ventral 3.5), using a glass pipette (~15  $\mu$ m diameter tip) connected to a nanoject II auto-nanoliter injector (Drummond Scientific) at a rate of 23 nl/s. For all injections, the pipette was left in place for 5 min before removing it from the brain. Mice were given analgesics (Carprofen; 5 mg/kg) and recovered for at least 2 d before their use in experiments. Mice that received different colored beads to label IT and PT neurons were anesthetized with a ketamine (100 mg/kg)/xylazine (10 mg/kg) mixture and were perfused through the heart with ice-cold saline consisting of the following (in mM): 2.5 KCl, 1.25 NaH<sub>2</sub>PO<sub>4</sub>, 25 NaHCO<sub>3</sub>, 0.5 CaCl<sub>2</sub>, 7 MgCl<sub>2</sub>, 7 dextrose, 205 sucrose, 1.3 ascorbate, and 3 sodium pyruvate (bubbled with 95% O<sub>2</sub>/5% CO<sub>2</sub> to maintain pH ~7.4) followed by 4% paraformaldehyde in 0.1 M phosphate buffer. Three hundred-micrometer-thick coronal slices were visualized with a Zeiss Axio Imager Z2 microscope running Axio Vision software (Carl Zeiss). We looked for clear instances of overlap of green and red puncta across at least four 300  $\mu$ m sections per animal.

### Slice preparation

Male WT and *fmr1*-/*y* mice, 8–16 weeks old, were anesthetized with a ketamine (100 mg/kg)/xylazine (10 mg/kg) mixture and were perfused through the heart with ice-cold saline consisting of the following (in mM): 2.5 KCl, 1.25 NaH<sub>2</sub>PO<sub>4</sub>, 25 NaHCO<sub>3</sub>, 0.5 CaCl<sub>2</sub>, 7 MgCl<sub>2</sub>, 7 dextrose, 205 sucrose, 1.3 ascorbate, and 3 sodium pyruvate (bubbled with 95% O<sub>2</sub>/5% CO<sub>2</sub> to maintain pH ~7.4). A vibrating tissue slicer (Vibratome 3000, Vibratome) was used to make 300- $\mu$ m-thick coronal sections. Slices were held for 30 min at 35°C in a chamber filled with artificial CSF (aCSF) consisting of the following (in mM): 125 NaCl, 2.5 KCl, 1.25 NaH<sub>2</sub>PO<sub>4</sub>, 25 NaHCO<sub>3</sub>, 2 CaCl<sub>2</sub>, 2 MgCl<sub>2</sub>, 10 dextrose, and 3 sodium pyruvate (bubbled with 95% O<sub>2</sub>/5% CO<sub>2</sub>) and then at room temperature until the time of recording.

### Electrophysiology

Recordings were made from L5 pyramidal neurons in the dorsal, medial prefrontal cortex ~1–2 mm anterior to bregma. Slices were placed in a submerged, heated (32–

Correspondence should be addressed to Brian E. Kalmbach, Center for Learning and Memory, The University of Texas at Austin, 1 University Station, C7000, Austin, TX 78712. E-mail: [brian@mail.clm.utexas.edu](mailto:brian@mail.clm.utexas.edu).

DOI:<http://dx.doi.org/10.1523/ENEURO.0114-15.2015>

Copyright © 2015 Kalmbach et al.

This is an open-access article distributed under the terms of the [Creative Commons Attribution 4.0 International](https://creativecommons.org/licenses/by/4.0/), which permits unrestricted use, distribution and reproduction in any medium provided that the original work is properly attributed.

34°C) recording chamber that was continually perfused (1 – 2 ml/min) with bubbled aCSF containing the following (in mM): 125 NaCl, 3.0 KCl, 1.25 NaH<sub>2</sub>PO<sub>4</sub>, 25 NaHCO<sub>3</sub>, 2 CaCl<sub>2</sub>, 1 MgCl<sub>2</sub>, 10 dextrose, 3 sodium pyruvate, 0.025 D-APV, 0.02 DNQX, 0.005 CGP, and 0.002 gabazine. For outside-out recordings, 0.001 mM TTX was added to the aCSF. Slices were viewed with either: (1) a Zeiss Axioskop microscope and differential interference optics, (2) a Zeiss AxioExaminer D microscope and Dodt contrast optics, or (3) a two-photon laser-scanning microscope (Leica SP5 RS) using Dodt contrast. Fluorescent-labeled neurons were visualized using a mercury lamp and a 540/605 nm or 470/502 nm excitation/emission filter set or two-photon excitation at 840 nm. Patch pipettes (4–8 M $\Omega$ ) were pulled from borosilicate glass and wrapped with Parafilm to reduce capacitance. The pipette solution for all configurations contained the following (in mM): 120 K-gluconate, 16 KCl, 10 HEPES, 8 NaCl, 7 K<sub>2</sub> phosphocreatine, 0.3 Na-GTP, 4 Mg-ATP, pH 7.3 with KOH. Neurobiotin (Vector Laboratories; 0.1%) was also included for histologic processing. For all experiments involving dendritic recordings and some experiments involving somatic recordings, AlexaFluor 594 (16  $\mu$ M; Invitrogen) was also included in the internal recording solution to determine the recording location. All drugs were prepared from concentrated stock solutions in water and were obtained from Abcam Pharmaceutical or Tocris.

### Whole-cell recordings

Data were acquired using a Dagan BVC-700 (Dagan) amplifier and custom data acquisition software written using Igor Pro (Wavemetrics) or AxoGraph X (AxoGraph Scientific) data acquisition software. Data were acquired at 10 – 50 kHz, filtered at 5 – 10 kHz, and digitized by an ITC-18 (InstruTech) interface. Pipette capacitance was compensated and the bridge was balanced during each recording. Series resistance was monitored throughout each experiment and was 10 – 25 M $\Omega$  for somatic recordings and 15 – 40 M $\Omega$  for dendritic recordings. Voltages are not corrected for the liquid-junction potential (estimated as  $\sim$ 12 mV).

Data were analyzed using either custom analysis software written in Igor Pro or using AxoGraph X. Subthreshold membrane properties were measured at a common membrane potential ( $-65$  mV). Input resistance ( $R_N$ ) sag and rebound were calculated from the voltage response to a family of 1000 ms current injections ( $-150$  to  $+50$  pA, 20 pA steps). Input resistance ( $R_N$ ) was calculated from the linear portion of the current–voltage relationship. Voltage sag was defined as the ratio of maximum to steady-state  $R_N$ . Rebound slope was calculated from the slope of the rebound amplitude as a function of steady-state membrane potential. The functional membrane time constant was defined as the slow component of a double-exponential fit of the average voltage decay in response to hyperpolarizing current injections (100 – 300 pA, 2 ms). Resonance was determined from the voltage response to a constant amplitude sinusoidal current injection that linearly increased in frequency from 1 – 15 Hz in 15 s. The impedance amplitude profile (ZAP) was constructed from

the ratio of the fast Fourier transform of the voltage response to the fast Fourier transform of the current injection. The peak of the ZAP was defined as the resonant frequency. Single action potentials (APs) were elicited using just-threshold current injections of various durations. AP threshold was defined as the voltage where the first derivative first exceeded 20 mV/ms. Simulated synaptic currents were generated with exponentially rising (dendrite = 0.2 ms; soma = 0.3 ms) and decaying (dendrite = 2 ms; soma = 4 ms) waveforms. The amplitude of this waveform was adjusted such that amplitude of the voltage response to a single simulated event was  $\sim$ 3 mV. For recordings from non-labeled neurons, the presence ( $>2.2$  Hz) or absence of resonance was used to classify neurons into projection types.

### Outside-out recordings

Membrane currents were recorded using an Axopatch 200B amplifier (Molecular Devices), sampled at 10 kHz, analog filtered at 2 kHz and digitized by an ITC-18 interface connected to a computer running Axograph X. For K<sup>+</sup> channels, activation curves were constructed by using depolarizing voltage commands ( $-70$  to  $50$  mV in 20 mV steps) to activate  $I_K$  from a holding potential of  $-90$  mV. Activation data were fit to a single Boltzmann function using a least-squares program. For voltage commands more hyperpolarized than  $-10$  mV, we extrapolated the slow time constant of the current back to the time equal to the peak of the total current. In this way, the peak of the slow and fast inactivating currents could be separated. The accuracy of this procedure was confirmed using a small set of experiments where the slowly inactivating component was measured directly. Linear leakage and capacitive currents were digitally subtracted by scaling traces at smaller command voltages in which no voltage-dependent current was activated.

### Data analysis

Repeated-measures (RM) ANOVA, between-subject factors ANOVA, mixed factors ANOVA, and *post hoc t* tests were used to test for statistical differences between experimental conditions. Bonferroni correction was used to correct for multiple comparisons. Pearson's product moment correlation was used to test for statistically significant correlations between variables. Error bars represent SEM. Statistical analyses were performed Prism (Graphpad). Data are presented in the text as mean  $\pm$  SEM.

## Results

### The organization of L5 projection neurons is maintained in the *fmr1-/-* mouse PFC

Testing for differences in ion channel function is complicated by heterogeneity in pyramidal neuron types within PFC. Pyramidal neurons are present throughout L2–6 and possess distinct morphology, connectivity, and repertoires of ion channels (Molyneaux et al., 2007; Shepherd, 2013; Dembrow and Johnston, 2014). For example, in L5, neurons projecting solely within the telencephalon (IT) possess distinct morphologic and physiologic prop-

erties from those of neighboring neurons that project subcortically through the PT (Christophe et al., 2005; Molnár and Cheung, 2006; Hattox and Nelson, 2007; Dembrow et al., 2010; Morishima et al., 2011; Otsuka and Kawaguchi, 2011; Sheets et al., 2011; Avesar and Gullledge, 2012; Gee et al., 2012; Kalmbach et al., 2013; Lee et al., 2014).

Before testing for alterations to physiology, we first asked whether the two general types of L5 projection neurons are found in the *fmr1*-/*yl* mouse medial PFC (mPFC). In WT and *fmr1*-/*yl* mice, we infused red retrograde tracer (Lumuf flour beads) into the pontine nuclei to label PT neurons and a green tracer into either the contralateral striatum or contralateral mPFC to label IT neurons. In both genotypes, IT neurons were found throughout L2–6, whereas PT neurons were restricted to L5/6. Within the deep layers, PT and IT neurons could be observed within close proximity to each other at all depths ( $<20 \mu\text{m}$ ). Furthermore, we did not observe clearly any double-labeled neurons in either genotype ( $n = 2$  for each genotype; Fig. 1A). Together, these data suggest that in *fmr1*-/*yl* mice, as in WT mice, IT and PT neurons represent two non-overlapping populations of neurons.

As an additional test, we next asked whether L5 IT and PT neurons in *fmr1*-/*yl* mice could be distinguished based upon their physiologic properties. PT neurons possess conductances that endow them with membrane resonance in the 3–7 Hz range whereas IT neurons are non-resonant. Thus, the presence of resonance can be used to distinguish PT from IT neurons (Dembrow et al., 2010). For these experiments, we made whole-cell current-clamp recordings from the soma of identified L5 PT or IT neurons, as well as nearby unlabeled cells. In both WT ( $n = 15$  cells from 6 mice,  $4.11 \pm 0.32$  Hz) and *fmr1*-/*yl* ( $n = 21$  cells from 7 mice,  $2.79 \pm 0.19$  Hz) mice, PT neurons displayed membrane resonance whereas IT neurons did not (WT:  $n = 17$  cells from 5 mice,  $1.07 \pm 0.06$  Hz; *fmr1*-/*yl*:  $n = 19$  cells from 6 mice,  $1.01 \pm 0.01$  Hz; IT vs PT,  $p < 0.001^a$ , ANOVA; Fig. 1B,C; Table 1). Furthermore, in both genotypes, input resistance ( $R_N$ ) was significantly higher in PT compared with IT neurons (WT PT =  $79.53 \pm 6.65$  M $\Omega$ ; WT IT =  $112.90 \pm 11.78$  M $\Omega$ ; *fmr1*-/*yl* PT =  $89.04 \pm 5.21$  M $\Omega$ , *fmr1*-/*yl* IT  $171.3 \pm 8.73$  M $\Omega$ ;  $p < 0.001^b$ , ANOVA; Fig. 1B,C). We also recorded from non-resonant (WT:  $n = 3$  cells from 2 mice; *fmr1*-/*yl*:  $n = 3$  from 2 mice) and resonant (WT:  $n = 13$  from 4 mice; *fmr1*-/*yl*:  $n = 11$  cells from 3 mice) non-labeled neurons with physiologic properties that closely resembled nearby labeled IT and PT neurons, respectively. When these putative IT and PT neurons were grouped with labeled projection neurons for analysis, we found that in both genotypes, PT neuron resonant frequency was inversely correlated with  $R_N$ , whereas in IT neurons it was not (Fig. 1C; WT PT:  $r^2 = 0.22$ ,  $p = 0.01^c$ ; WT IT:  $r^2 = 0.01$ ,  $p = 0.62$ ; *fmr1*-/*yl* PT:  $r^2 = 0.12$ ,  $p = 0.05$ , *fmr1*-/*yl* IT:  $r^2 = 0.08$ ,  $p = 0.18$ ). These data are consistent with findings in rat mPFC (Dembrow et al., 2010) and suggest that the organization of projection neurons in L5 of PFC is maintained in the *fmr1*-/*yl* mouse. For our purposes, unlabeled neurons that display

resonance will be referred to as PT neurons, whereas those that do not will be referred to as IT neurons.

### $I_h$ is reduced in L5 neurons in the *fmr1*-/*yl* mouse mPFC

The intrinsic membrane properties of pyramidal neurons are heavily influenced by the presence of voltage-gated ion channels (Magee, 2000; London and Häusser, 2005; Johnston and Narayanan, 2008). The expression of one class of channel, h-channels, which carry  $I_h$ , has been reported to be up-regulated in CA1 but down-regulated in somatosensory cortex in the *fmr1*-/*yl* mouse (Brager et al., 2012; Zhang et al., 2014).

To test for alterations to h-channel function in PFC we measured  $I_h$ -sensitive membrane properties (membrane potential –  $V_m$ ,  $R_N$ , time constant – tau, sag, rebound, resonance, and temporal summation; Hutcheon and Yarom, 2000; Robinson and Siegelbaum, 2003; Brager and Johnston, 2007; Narayanan and Johnston, 2007) in WT and *fmr1*-/*yl* neurons. Because h-channel expression in many types of cortical pyramidal neurons increases with distance from the soma (Lörincz et al., 2002; Kole et al., 2006), we performed these measurements at the soma (WT:  $n = 30$  cells from 18 mice; *fmr1*-/*yl*:  $n = 35$  cells; from 17 mice), proximal dendrite ( $\leq 250 \mu\text{m}$ ; WT:  $n = 12$  cells from 9 mice; *fmr1*-/*yl*:  $n = 17$  cells from 17 mice), and distal dendrite ( $>250 \mu\text{m}$ ; WT:  $n = 34$  cells from 26 mice; *fmr1*-/*yl*:  $n = 23$  cells from 17 mice). We focused our initial efforts on PT neurons because they have more pronounced h-channel associated properties (Fig. 1; Dembrow et al., 2010; Sheets et al., 2011; Kalmbach et al., 2013).  $R_N$  was higher at proximal and distal dendritic recording locations ( $p < 0.01^d$ ) in *fmr1*-/*yl* compared with WT neurons, but this difference was not observed at the soma ( $p = 0.21$ ; Fig. 2A,B). *Fmr1*-/*yl* neurons were more hyperpolarized, displayed less sag and less rebound than WT neurons, at all recording locations (all  $p < 0.01$ ; Fig. 2A,B<sup>e</sup>). Furthermore, the resonant frequency of *fmr1*-/*yl* neurons was lower and the functional membrane time constant longer than WT neurons at all recording locations ( $p < 0.01$ ; Fig. 2C,D<sup>f</sup>). Finally, *fmr1*-/*yl* neurons displayed greater temporal summation of simulated synaptic currents at both the soma and distal dendritic recording locations ( $p < 0.001$ , ANOVA; Fig. 2E<sup>g</sup>). Together, these differences in membrane properties between genotypes suggest that there is a decrease in  $I_h$  at both the soma and dendrite of L5 PT neurons in PFC of *fmr1*-/*yl* mice.

To test for differences in IT neurons, we made many of these same measurements at the soma (WT:  $n = 20$  cells from 8 mice; *fmr1*-/*yl*:  $n = 22$  cells from 10 mice) and dendrite (WT:  $n = 7$  cells from 7 mice; 125–270  $\mu\text{m}$ ,  $192.86 \pm 17.52 \mu\text{m}$  from soma; *fmr1*-/*yl*:  $n = 8$  cells from 8 mice; 145–300  $\mu\text{m}$ ,  $235 \pm 20.28 \mu\text{m}$  from soma). In contrast to PT neurons, the subthreshold properties of IT neurons were largely similar in WT and *fmr1*-/*yl* mice (all comparisons  $p > 0.1$ ; ANOVA; Fig. 3<sup>h</sup>). The lone exception was resting membrane potential (RMP) where *fmr1*-/*yl* neurons were more hyperpolarized compared with WT neurons ( $p = 0.02$ ; ANOVA; Fig. 3A<sup>i</sup>). Differences in RMP

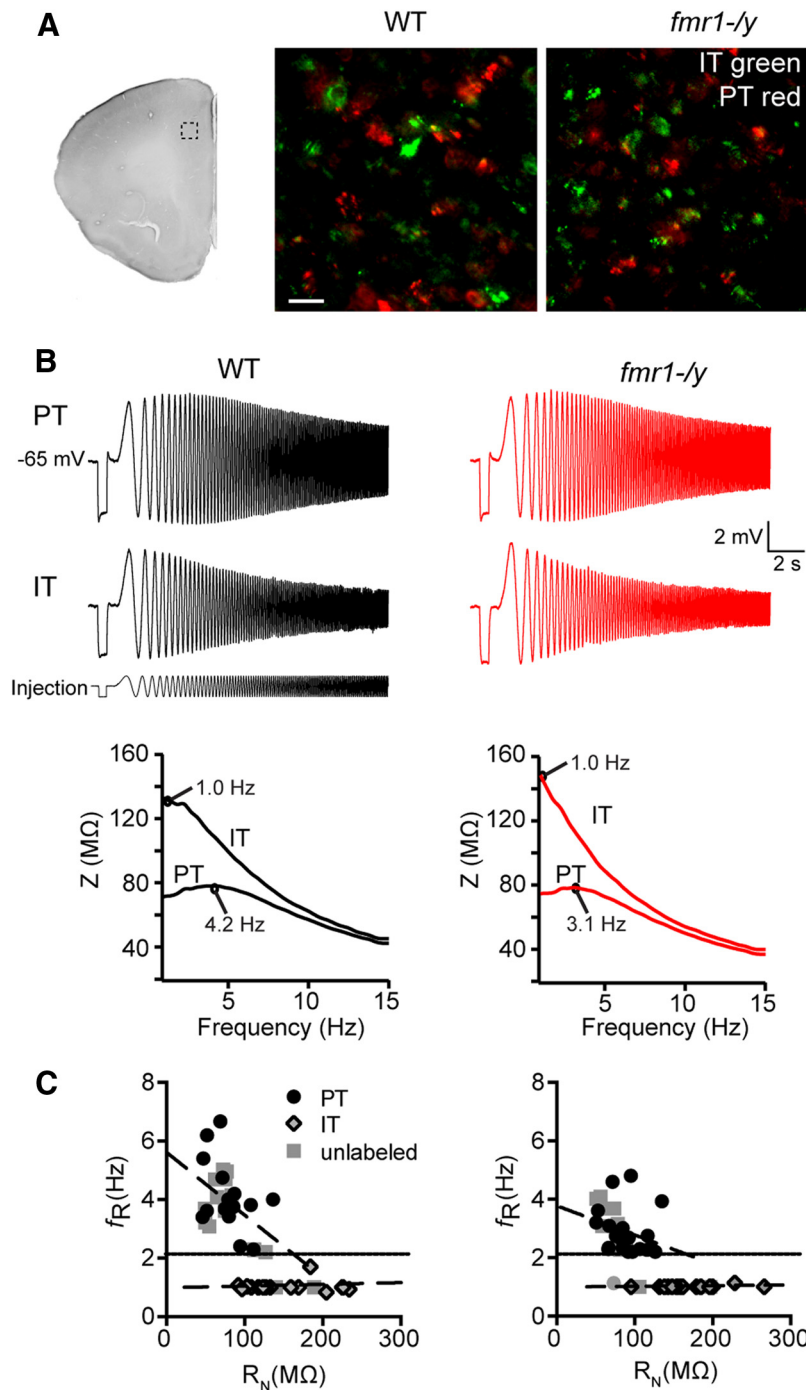


**Figure 1. PT and IT neurons in L5 of mPFC in the *fmr1-/-* mouse.** **A**, Coronal section of one hemisphere of mouse mPFC illustrating approximately where neurons were visualized. Retrograde labeled IT and PT neurons in the middle of L5 in WT (left) and *fmr1-/-* mouse mPFC. IT (green) and PT (red) neurons were non-overlapping populations of neurons in both genotypes. Scale bar, 20  $\mu$ m. **B**, Response to a chirp current injection in WT (left) and *fmr1-/-* (right) PT and IT neurons and the resultant ZAP for each neuron. **C**, IT and PT neurons were distinguishable based on intrinsic membrane properties in both genotypes. In both genotypes, PT neurons were resonant, whereas IT neurons were non-resonant.  $f_R$  in PT neurons was negatively correlated with  $R_N$  in both genotypes ( $p < 0.05$ ).

at the soma persisted in the presence of the h-channel blocker ZD7288 (10  $\mu$ M; WT:  $n = 6$  cells from 4 mice baseline  $-64.33 \pm 1.50$  ZD7288  $-68.52 \pm 0.23$ ; *fmr1-/-*:  $n = 6$  cells from 4 mice baseline  $-69.63 \pm 1.56$  ZD7288

$-72.15 \pm 1.48$ ;  $p = 0.04$ ; ANOVA), suggesting that h-channels were not the main source of these differences.

To test whether the observed differences in PT neurons were due primarily to h-channels, we compared the ef-

Table 1. Statistical Tests

	Data	Test	Measurement/group	Power	Effect size
a	Unknown	ANOVA		100	3.28
b	Normal	ANOVA		100	1.21
c	Normal	Pearson correlation	WT PT	65.6	0.28
	Unknown	Pearson correlation	WT IT	6.3	0.01
	Normal	Pearson correlation	<i>fmr1-ly</i> PT	40.9	0.14
	Unknown	Pearson correlation	<i>fmr1-ly</i> IT	19	0.09
d	Normal	<i>t</i> test	RN distal	94.5	0.98
	Normal	<i>t</i> test	RN proximal	84.5	1.14
	Normal	<i>t</i> test	RN soma	23.2	0.31
e	Unknown	ANOVA	Rebound	98.3	0.37
	Unknown	ANOVA	Sag	99.6	0.39
	Normal	ANOVA	RMP	97.6	0.33
f	Unknown	ANOVA	Resonance	99.9	0.47
	Normal	ANOVA	tau	99.8	0.43
g	Normal	ANOVA	Soma	94	0.79
	Normal	ANOVA	Dendrite	97	0.74
h	Normal	ANOVA	Rn	36	0.22
	Unknown	ANOVA	Sag	12.6	0.11
	Unknown	ANOVA	Rebound	43	0.24
i	Unknown	ANOVA	Resonance	6.5	0.05
	Normal	ANOVA		67.2	0.33
	Normal	ANOVA		55.2	0.71
j	Unknown	<i>t</i> test	RN	18.1	0.73
	Unknown	<i>t</i> test	Sag	2.5	0
	Unknown	<i>t</i> test	Rebound	11.3	0.57
	Unknown	<i>t</i> test	Resonance	10.4	0.54
	Unknown	<i>t</i> test	tau	18.2	0.73
	Unknown	<i>t</i> test	RMP	2.9	0.13
	Unknown	<i>t</i> test	Summation	6.2	0.38
l	Unknown	ANOVA	5.3	0.08	
m	Unknown	<i>t</i> test		98.8	4.80
n	Unknown	<i>t</i> test		96.1	1.77
o	Normal	ANOVA	99.9	0.93	
	Normal	<i>t</i> test	94.7	1.50	
p	Normal	<i>t</i> test	/KA-fast	77.9	1.50
	Normal	<i>t</i> test	/K-sustained	60.4	1.35
q	Unknown	<i>t</i> test	/KA-fast	8.1	0.55
	Unknown	<i>t</i> test	/K-sustained	3.1	0.21
r	Normal	<i>t</i> test	/KA-fast soma vs dend <i>fmr1-ly</i>	79.6	1.74
	Normal	<i>t</i> test	/KA-fast soma vs dend WT	3.6	0.23
	Normal	<i>t</i> test	/K-sustained soma v dend <i>fmr1-ly</i>	72.5	1.72
	Normal	<i>t</i> test	/K-sustained soma vs dend WT	8.67	0.58
s	Normal	<i>t</i> test	WT soma v dend	92.1	2.20
	Normal	<i>t</i> test	KO soma v dend	86.6	1.99
t	Normal	<i>t</i> test		51.5	1.14
u	Normal	<i>t</i> test		5.4	0.03
	Normal	ANOVA	/K-total	27.4	0.27
	Normal	ANOVA	/KA-fast	8.4	0.11
	Normal	ANOVA	/K-sustained	9.2	0.13
	Normal	ANOVA	/K-slow	13.8	0.19
v	Normal	ANOVA		85	2.07
w	Unknown	<i>t</i> test		99.2	0.20
x	Unknown	<i>t</i> test		26.5	0.30
y	Normal	ANOVA		10	0.15
z	Normal	ANOVA		100	2.02
a'	Unknown	ANOVA	4-AP		
b'	Unknown	ANOVA	100		5.20
Unknown	ANOVA	$\alpha$ DTX			
c'	Unknown	ANOVA		100	3.74
d'	Unknown	<i>t</i> test		54	1.76
e'	Unknown	<i>t</i> test		3	0.20
f'	Unknown	ANOVA		7.7	0.12
g'	Normal	ANOVA		100	1.50
h'	Normal	<i>t</i> test		12	71
l'	Normal			24	93

	Data	Test	Measurement/group	Power	Effect size
j'	Normal			50	88.9
k'	Normal			100	81.9
	Normal			100	0.51
	Normal	ANOVA		71.2	0.18
	Normal	ANOVA		62.6	0.21
k'	Normal	ANOVA	WT	99.9	0.90
l'	Normal		<i>fmr1-ly</i>	94.3	0.61
m'	Normal	ANOVA		99.9	0.81
n'	Normal	ANOVA		99.9	0.75
	Normal	ANOVA	WT	10	0.14
o'	Normal	ANOVA	<i>fmr1-ly</i>	17.78	0.19
p'	Normal	ANOVA		99.9	1.03
q'	Normal	ANOVA		92.2	0.38

Data structure was tested for normality using Kolmogorov–Smirnov tests. In cases where the test for normality failed, nonparametric statistic yielded similar results. For some comparisons, the measurement and/or group under comparison is listed for clarity. *Post hoc* power analysis was performed using G × Power (v3.1.9.2, [www.Gpower.hhu.de](http://www.Gpower.hhu.de)).

effects of the ZD7288 on the properties of PT L5 dendrites in WT versus *fmr1-ly* mice. Application of 10 μM ZD7288 largely eliminated the differences in membrane properties between WT (*n* = 7 cells from 6 mice) and *fmr1-ly* (*n* = 9 cells from 7 mice) neurons measured at a common membrane potential (−65 mV; Fig. 4). There were no statistical differences in  $R_N$  ( $p$  = 0.12),  $V_m$  ( $p$  = 0.94), sag ( $p$  = 0.40), rebound ( $p$  = 0.08; Fig. 4A,B), resonant frequency ( $p$  = 0.37; Fig. 4C), tau ( $p$  = 0.18; Fig. 4D), or temporal summation of simulated synaptic input ( $p$  = 0.30; Fig. 4E) in

the presence of ZD7288 in WT versus *fmr1-ly* neurons (all *post hoc* comparisons<sup>k</sup>).

Finally, we made outside-out patch-clamp recordings from the distal dendrite of PT neurons to directly compare  $I_h$  in WT (*n* = 4 cells from 3 mice; 225–400 μm, 340 ± 37.6 μm from soma) and *fmr1-ly* (*n* = 5 cells from 5 mice; 250–350, 308 ± 17.7 μm from soma) mice. Voltage steps from a holding potential of −30 to −140 mV elicited an inward current in both genotypes (Fig. 5A). The activation of this current was well fit by a double-exponential. The

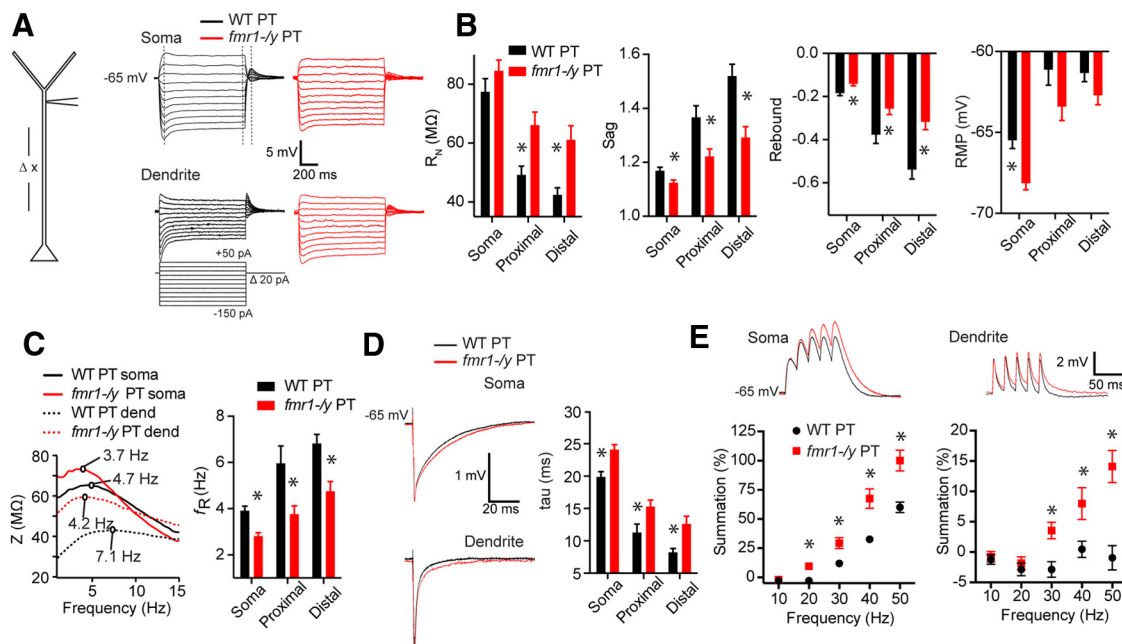


**Figure 2. Altered h-dependent membrane properties in L5 PT neurons of mPFC in the *fmr1-ly* mouse.** **A**, Left, Whole-cell recordings were made at various distances from the soma in WT and *fmr1-ly* mouse PT neurons. Right, Example traces from whole-cell recordings from the soma and dendrite of WT and *fmr1-ly* neurons in response to the current injection shown below. All recordings were made at −65 mV. **B**,  $R_N$  was higher in the dendrite, but not soma of *fmr1-ly* neurons compared with WT. In addition, *fmr1-ly* neurons were more hyperpolarized and displayed less sag and rebound at the soma and dendrite compared with WT neurons. **C**, *fmr1-ly* neurons displayed a lower resonant frequency at the soma and dendrite compared with WT neurons. Sample ZAPs are shown at right. **D**, The functional membrane time constant was longer in *fmr1-ly* compared with WT neurons, at all recording sites. **E**, *fmr1-ly* neurons displayed greater temporal summation of simulated synaptic currents compared with WT neurons at the soma and distal dendritic recording locations. \* $p$  < 0.01, *post hoc* comparison across genotypes.

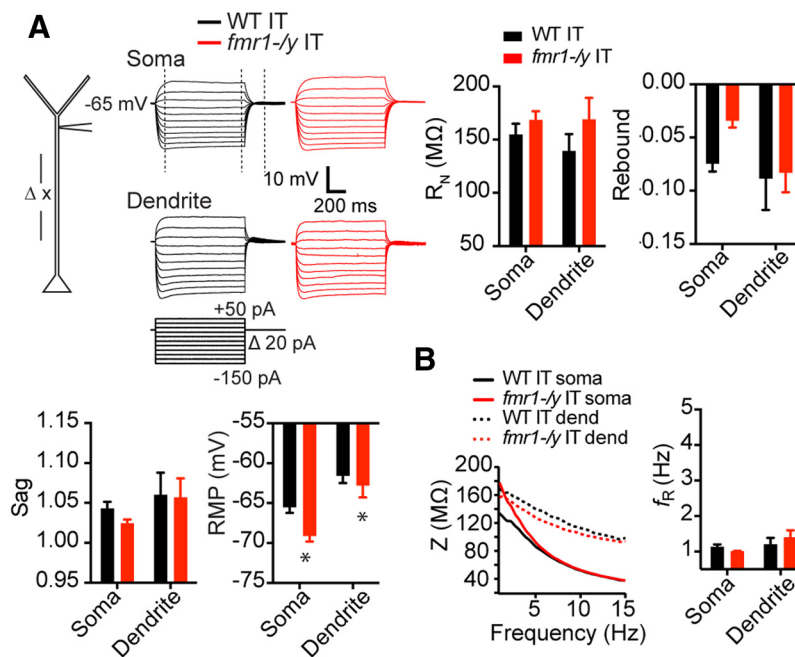


**Figure 3. Subthreshold membrane properties are largely unaltered in IT neurons of PFC in the *fmr1-ly* mouse.** **A**, Left, Whole-cell recordings were made at various distances from the soma in WT and *fmr1-ly* mouse IT neurons. Right, Example traces from whole-cell recordings from the soma and dendrite of WT and *fmr1-ly* neurons in response to the current injection shown below. All recordings were made at  $-65$  mV.  $R_N$ , sag, and rebound were not different at the soma or dendrite in *fmr1-ly* compared with WT IT neurons. RMP was hyperpolarized in *fmr1-ly* compared with WT IT neurons. **B**, *fmr1-ly* and WT IT neurons both displayed a similar resonant frequency at the soma and dendrite. \* $p < 0.05$ , *post hoc* comparison across genotypes.

fast and slow time constants were not different between genotypes and both were consistent with  $I_h$  (Fig. 5B;  $p = 0.87$ , mixed-ANOVA; Dougherty et al., 2013). The maximum dendritic  $I_h$  was greater in WT compared with *fmr1-ly* neurons (Fig. 5C;  $p = 0.001$ , *t* test<sup>m</sup>). Finally, the resonant frequency measured during whole-cell before obtaining the outside-out configuration was lower in *fmr1-ly* compared with WT dendrites (Fig. 5D;  $p = 0.03$ , *t* test<sup>n</sup>). These data are consistent with a decrease in the functional expression of h-channels in L5 PT neurons of PFC in the *fmr1-ly* mouse.

#### Alterations to $I_K$ in L5 mPFC pyramidal neurons in *fmr1-ly* mice

The observed decrease in  $I_h$  in PT neurons is in contrast to pyramidal neurons in CA1 of the hippocampus (Brager et al., 2012), but is similar to L5 pyramidal neurons in somatosensory cortex (Zhang et al., 2014). Together, these observations suggest that the absence of FMRP can have divergent effects on channel expression/function depending upon brain region or neuron type. A-type  $K^+$  and h-channel function are affected in opposite directions by several manipulations (Harris-Warrick et al., 1995; Bernard et al., 2004; Frick et al., 2004; Fan et al., 2005; Shin et al., 2008). Thus, we next asked whether the functional expression of A-type  $K^+$  channels, which is decreased in CA1 pyramidal neurons in the *fmr1-ly* mouse (Routh et al., 2013), is increased in L5 neurons of mPFC and if so, whether the change is restricted to one class of L5 projection neuron.

We used outside-out patch recordings to measure the total  $K^+$  current at the soma and distal dendrite ( $\geq 250$   $\mu$ m) of PT L5 neurons in WT and *fmr1-ly* mice (Fig. 6A). The current elicited by step depolarization to 50 mV from a holding potential of  $-90$  mV contained both a transient and a sustained component ( $I_{K-total}$ ; Fig. 6A1). Macroscopic  $K^+$  currents in L5 neurons in granular cortex are composed of distinct channels with fast and slow inactivation kinetics (Bekkers, 2000; Korngreen and Sakmann, 2000). To test whether PT neurons in mPFC possess similar diversity in  $K^+$  currents, we used the voltage-dependent properties of the putative channels underlying each of these components to isolate the individual currents. A brief (100 ms) prepulse to  $-20$  mV was used to inactivate the fast-inactivating current without significantly affecting either the sustained or slowly inactivating current (Fig. 6A2). Subtracting the resulting current from total  $I_K$  revealed a rapidly inactivating  $K^+$  current ( $I_{KA-fast}$ ; Fig. 6A4). Step depolarization to 50 mV from a holding potential of  $-20$  mV, to inactivate all transient  $K^+$  currents, revealed a sustained current ( $I_{K-sustained}$ ; Fig. 6A3). Subtracting  $I_{K-sustained}$  from the current in Fig. 6A2 revealed a slowly inactivating  $K^+$  current ( $I_{K-slow}$ ; Fig. 6A5). Thus, we were able to isolate three kinetically distinct outward currents:  $I_{K-sustained}$ ,  $I_{KA-fast}$ , and  $I_{K-slow}$  (Fig. 6A).

The maximum  $I_{K-total}$  was greater at the soma compared with the dendrite for WT and *fmr1-ly* neurons ( $p < 0.001$ , ANOVA). However, the maximum somatic  $I_{K-total}$  in *fmr1-ly* neurons was larger than that in WT neurons ( $p = 0.01$ ; Fig. 6B<sup>p</sup>). This difference in somatic  $I_{K-total}$  is due, in part, to

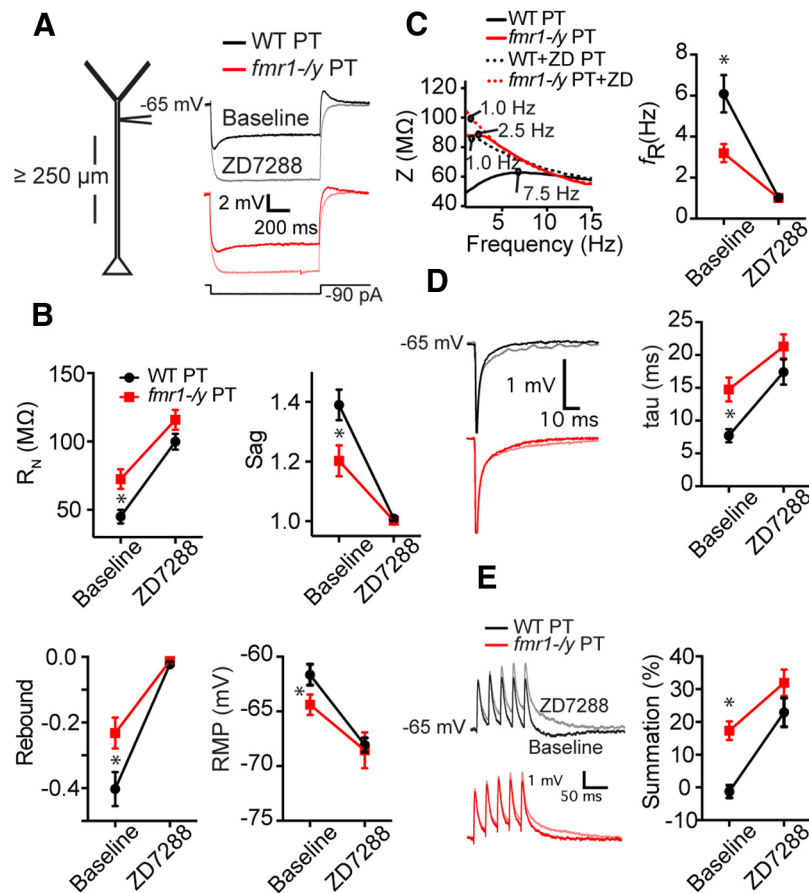


**Figure 4. Differences in membrane properties between WT and *fmr1-/-* neurons are eliminated by the h-channel blocker, ZD7288.** **A**, Sample voltage responses to a hyperpolarizing current injection at the distal dendrite of *fmr1-/-* and WT PT neurons. **B**, ZD7288 (10  $\mu\text{M}$ ) eliminated differences in  $R_N$ , Sag, rebound and RMP between WT and *fmr1-/-* dendrites. **C**, ZD7288 also eliminated membrane resonance in both genotypes. **D**, The functional membrane time constant and temporal summation of simulated synaptic currents delivered at 50 Hz (**E**) was no different between *fmr1-/-* and WT dendrites in the presence of ZD7288. All measurements were performed at  $-65\text{ mV}$ .  $*p < 0.01$ .

differences in both  $I_{K_{A\text{-fast}}}$  and  $I_{K_{\text{sustained}}}$ . We observed larger  $I_{K_{A\text{-fast}}}$  and  $I_{K_{\text{sustained}}}$  at the soma ( $p = 0.05$ ; fast,  $p = 0.05^{\text{a}}$ ) but not dendrite (sustained,  $p = 0.74$ ; fast,  $p = 0.52^{\text{a}}$ ), of *fmr1-/-* compared with WT neurons (Fig. 6C,E). Consequently,  $I_{K_{A\text{-fast}}}$  ( $p < 0.01$ ) and  $I_{K_{\text{sustained}}}$  ( $p < 0.05$ ) were larger at the soma compared with the dendrite in *fmr1-/-*, but not WT neurons (Fig. 6C,E<sup>s</sup>). Interestingly, we also observed genotypic differences for the  $I_{K_{\text{slow}}}$ .  $I_{K_{\text{slow}}}$  was smaller at the dendrite compared with the soma in both genotypes ( $p < 0.05^{\text{a}}$ ). In contrast to the other currents however,  $I_{K_{\text{slow}}}$  was smaller at the soma of *fmr1-/-* compared with WT neurons ( $p < 0.05$ ; Fig. 6D<sup>u</sup>). In summary, at the soma of *fmr1-/-* PT neurons, there is a relative increase in the contribution of  $I_{K_{A\text{-fast}}}$  ( $57 \pm 3\%$  vs  $44 \pm 7\%$ ) and decrease in the contribution of  $I_{K_{\text{slow}}}$  ( $50 \pm 6\%$  vs  $36 \pm 3\%$ ) to the somatic  $I_{K_{\text{total}}}$  compared with WT (Fig. 6F). In contrast, we observed no differences between genotypes in relative contribution of the three  $K^+$  current components in the dendrites (Fig. 6G).

Relatively little is known about differences in  $K^+$  channel expression at the soma of different projection neurons in L5. Therefore, we also made outside-out patch record-

ings from IT neurons in mPFC to test whether the change in magnitude and relative contribution of  $K^+$  currents observed at the soma of PT neurons is common to all pyramidal neurons within a brain region. Similar to PT neurons, the current elicited by step depolarization to 50 mV from a holding potential of  $-90\text{ mV}$  contained both transient and sustained components. In contrast to PT neurons however, we did not observe differences in any  $I_K$  component between *fmr1-/-* and WT IT neurons at the soma or dendrite (Fig. 7;  $p > 0.05$ , all comparisons<sup>v</sup>). Thus, in the *fmr1-/-* mouse, the maximum amplitude of  $K^+$  currents at the soma is affected in one type of projection neuron (PT), but not a neighboring type (IT). These data suggest that channel phenotypes in the *fmr1-/-* mouse can vary not only between brain regions (ie, hippocampus, somatosensory cortex and mPFC), but also within a brain region in different classes of principal neurons (PT vs IT).

A-type  $K^+$  channels can be composed of either Kv4 or Kv1 subunits (Coetzee et al., 1999). To identify the putative channels underlying  $I_{K_{A\text{-fast}}}$  and  $I_{K_{\text{slow}}}$ , we used two complementary approaches. First, we exploited differ-

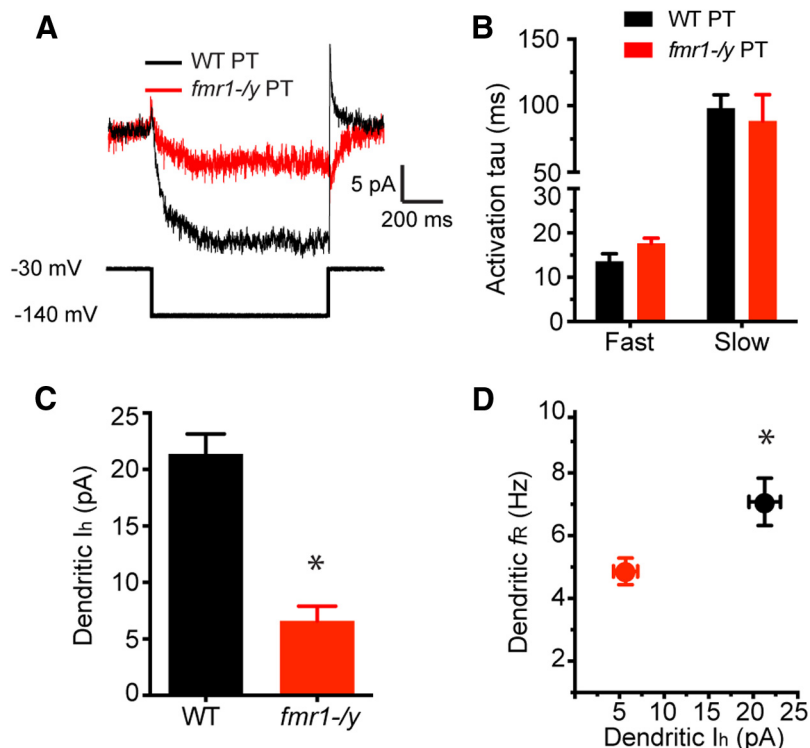
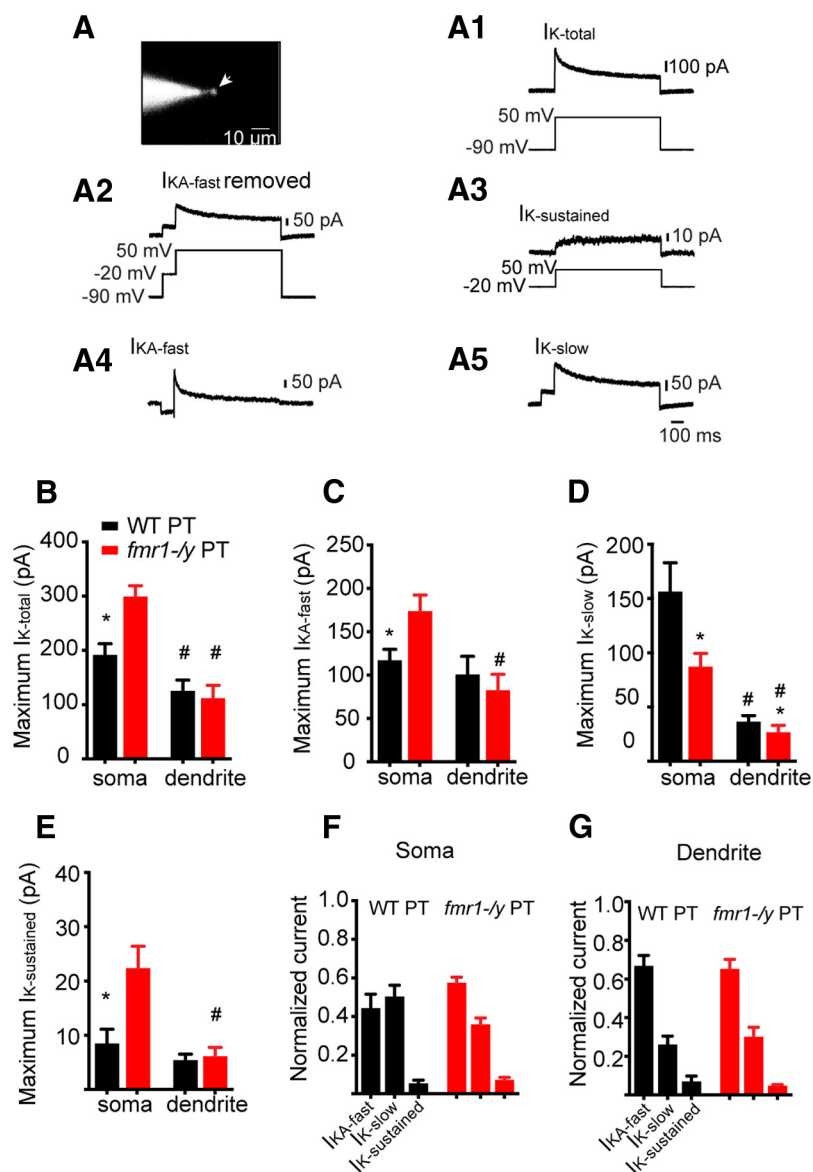


Figure 5.  $I_h$  is reduced in the dendrites of L5 PT neurons of PFC in the *fmr1-/-* mouse. **A**, h-Current was measured by stepping from a holding potential of  $-30$  mV to  $-140$  mV for 500 ms. **B**, There were no genotypic differences in the time constant of activation of  $I_h$ . **C**, Both  $I_h$  and resonance (**D**) were significantly reduced in the dendrite of *fmr1-/-* neurons compared with WT. \* $p < 0.05$

ences in the kinetic properties of these channels. Kv1 containing channels tend to inactivate and recover from inactivation an order of a magnitude slower than Kv4 containing channels (Castellino et al., 1995; Jerng et al., 2004). The time constant of inactivation ( $\tau_{\text{inactivation}}$ ) of the  $I_{\text{KA-fast}}$  was not different between WT and *fmr1-/-* for either PT (WT  $\tau_{\text{inactivation}} = 29$  ms; *fmr1-/-*  $\tau_{\text{inactivation}} = 25$  ms) or IT neurons (WT  $\tau_{\text{inactivation}} = 28$  ms; *fmr1-/-*  $\tau_{\text{inactivation}} = 23$  ms;  $p = 0.88$ , ANOVA<sup>W</sup>). These values were consistent with Kv4 channels. The  $\tau_{\text{inactivation}}$  of the  $I_{\text{K-slow}}$  was an order of magnitude larger than the  $\tau_{\text{inactivation}}$  of the  $I_{\text{KA-fast}}$  in both WT and *fmr1-/-* for PT and IT neurons, consistent with Kv1 channels. A closer comparison revealed that the  $\tau_{\text{inactivation}}$  of the  $I_{\text{K-slow}}$  in *fmr1-/-* PT neurons was significantly smaller compared with WT PT neurons (WT  $\tau_{\text{inactivation}} = 646 \pm 95$  ms; *fmr1-/-*  $\tau_{\text{inactivation}} = 244 \pm 44$  ms;  $p = 0.01^*$ ). By contrast, there was no statistically significant difference in  $\tau_{\text{inactivation}}$  for  $I_{\text{K-slow}}$  in IT neurons (WT  $\tau_{\text{inactivation}} = 630 \pm 100$  ms; *fmr1-/-*  $\tau_{\text{inactivation}} = 425 \pm 69$  ms;  $p > 0.05$ , Fig. 8A<sup>y</sup>). Next, we used a two-pulse protocol to measure the recovery from inactivation. We found that the time course of recovery from inactivation was well fit by two exponentials consistent with two types of transient K<sup>+</sup> channels. Both the fast ( $p = 0.2$ , ANOVA<sup>2</sup>) and slow ( $p = 0.5$ , ANOVA<sup>a</sup>) time constant of recovery from inactivation were similar in WT and *fmr1-/-* for L5 PT and IT neurons and were consistent with Kv4-containing and Kv1-containing channels, respectively (Fig. 8B–D).

As an additional method of identifying the channels underlying these currents, we exploited differences in the sensitivity of Kv1 and Kv4 containing channels to K<sup>+</sup> channel blockers. Specifically, we measured the sensitivity of macroscopic K<sup>+</sup> currents to 50  $\mu\text{M}$  4-aminopyridine (4-AP) and 150  $\mu\text{M}$  Ba<sup>2+</sup>, which preferentially block Kv1-containing and Kv4-containing channels, respectively (Castle et al., 1994; Russell et al., 1994; Stephens et al., 1994; Coetzee et al., 1999; Gasparini et al., 2007). Additionally, we measured the sensitivity of these currents to alpha-dendrotoxin ( $\alpha$ -DTX), which preferentially blocks Kv1.1-, 1.2-, and 1.6-containing channels (Harvey, 2001). 4-AP (50  $\mu\text{M}$ ) and  $\alpha$ -DTX (200 nM) decreased  $I_{\text{KA-slow}}$  without significantly affecting  $I_{\text{KA-fast}}$  ( $p < 0.01$ ,  $n = 8$  patches from 4 mice and  $p < 0.001$ ,  $n = 5$  patches from 4 mice, respectively; two-way RM ANOVA; Fig. 9A,B<sup>b</sup>). In contrast, 150  $\mu\text{M}$  Ba<sup>2+</sup> decreased  $I_{\text{KA-fast}}$  without significantly affecting  $I_{\text{KA-slow}}$  ( $p < 0.005$ ,  $n = 5$  patches from 3 mice; two-way RM ANOVA; Fig. 9C<sup>c</sup>). Furthermore, the amplitude of the DTX- and 4-AP-sensitive current was similar to the amplitude of  $I_{\text{KA-slow}}$ , whereas the amplitude of the Ba<sup>2+</sup>-sensitive current was similar to the amplitude of  $I_{\text{KA-fast}}$  (Fig. 9D). Together, these data suggest that Kv4 containing channels contribute to  $I_{\text{KA-fast}}$  and Kv1 containing channels contribute to  $I_{\text{K-slow}}$ . Thus, our data suggest that in the *fmr1-/-* mouse, there are alterations to the functional expression of two K<sup>+</sup> channels in PT L5 neurons of mPFC; there is an increase in the expres-



**Figure 6. Differences in  $I_K$  in PT neurons in *fmr1-/-* versus WT mice.** **A**, Outside-out patch from a PT neuron visualized through fluorescence microscopy.  $I_{K-total}$  was measured by stepping to +50 mV from a holding potential of -90 mV. A prepulse to -20 mV was used to inactivate fast inactivating  $I_{KA}$ .  $I_{K-sustained}$  was obtained by stepping from a holding potential of -20 mV to +50 mV.  $I_{KA-fast}$  was obtained by subtracting the current in **A2**, from the total current in **A1**.  $I_{K-slow}$  was obtained by subtracting the sustained current in **A3** from the current obtained in **A2**. **B**, Maximum  $I_{K-total}$  at the soma is greater in *fmr1-/-* PT neurons compared with WT neurons. **C**, Maximum  $I_{KA-fast}$  at the soma is greater in *fmr1-/-* neurons compared with WT. **D**, Maximum  $I_{K-slow}$  at the soma of *fmr1-/-* neurons is less compared with WT neurons. **E**, At the soma, maximum  $I_{K-sustained}$  is greater in *fmr1-/-* PT neurons compared with WT. **F**, Summary of somatic differences in  $I_K$  between WT and *fmr1-/-* neurons. **G**, There were no differences in dendritic  $K^+$  currents in *fmr1-/-* compared with WT neurons.

sion of Kv4-containing channels and a decrease in Kv1-containing channels.

In addition to a decrease in channel expression, there is a hyperpolarizing shift in the voltage dependence of activation of Kv4 channels in CA1 pyramidal neuron dendrites of *fmr1-/-* mice (Routh et al., 2013). Thus, although there is a decrease in total maximum current, there are relatively more channels open at hyperpolarized potentials in *fmr1-/-* mice compared with WT mice. To test for similar alterations to channel function in L5 neurons of mPFC, we

measured the voltage dependence of activation of fast A-type  $K^+$  channels in somatic and dendritic patches from WT and *fmr1-/-* mice (Fig. 8E). Consistent with published reports in granular cortex (Bekkers, 2000), there was a hyperpolarizing shift in the activation curve of  $I_{KA-fast}$  at the dendrite compared with the soma in WT L5 PT neurons ( $p = 0.03$ ; Fig. 8F,  $H^d$ ). In contrast, there was no such shift in *fmr1-/-* neurons ( $p = 0.76$ ; Fig. 8G,  $H^e$ ). Furthermore, there was no difference in slope factor between WT and *fmr1-/-* neurons at either recording location ( $p > 0.3^f$ ,

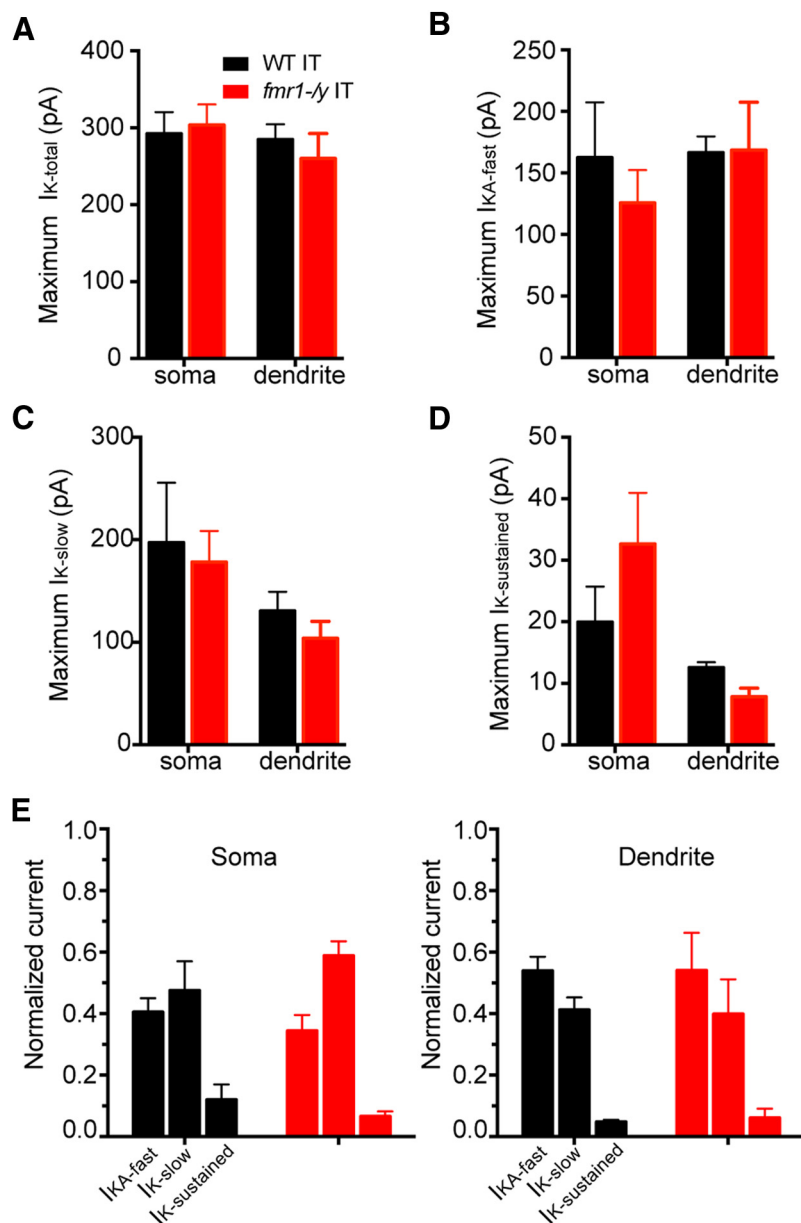


Figure 7.  $I_K$  is not different in IT neurons in *fmr1-/-* versus WT mice. At the soma and dendrite there were no differences in the maximum amplitude of (A)  $I_{K-total}$ , (B)  $I_{KA-fast}$ , (C)  $I_{K-slow}$ , or (D)  $I_{K-sustained}$  in *fmr1-/-* versus WT IT neurons. E, Summary of somatic and dendritic  $I_K$  in WT ( $n = 18$  somas from 12 mice and 5 dendrites from 5 mice; 180–330  $\mu\text{m}$ , 250  $\pm$  20.1  $\mu\text{m}$  from soma) and *fmr1-/-* IT ( $n = 11$  somas from 8 mice and 5 dendrites from 5 mice; 170–270  $\mu\text{m}$ , 215  $\pm$  27.7  $\mu\text{m}$  from soma) neurons.

ANOVA). Thus, the hyperpolarizing shift in the activation of  $I_{KA-fast}$  normally observed from soma to dendrite in WT neurons is absent in *fmr1-/-* neurons. These data suggest that although there is no difference in maximum  $I_{KA-fast}$  in the dendrites of *fmr1-/-* versus WT PT neurons, there may be subtle differences in voltage dependence of activation.

#### Altered action potential generation in *fmr1-/-* L5 PT neurons of mPFC

$K^+$  channels modulate several aspects of neural function, including the dynamics of action potential threshold. Changes to threshold, also known as threshold accommodation, can be mediated through the recruitment of  $K^+$

channels, in addition to  $Na^+$  channel inactivation (Hodgkin and Huxley, 1952). Kv4 and Kv1 subunits have both been implicated in regulating neural excitability by setting the threshold for action potential generation (Bekkers and Delaney, 2001; Kim et al., 2005; Higgs and Spain, 2011; Carrasquillo et al., 2012). Because we observed somatic differences consistent with alterations to these two  $K^+$  channels, we predicted that threshold dynamics would be altered in L5 PT neurons in mPFC.

To test this hypothesis, we injected current of varied duration at the soma of L5 PT neurons in both genotypes (WT:  $n = 20$  cells from 11 mice; *fmr1-/-*:  $n = 23$  cells from 9 mice). The current amplitude for a given duration was

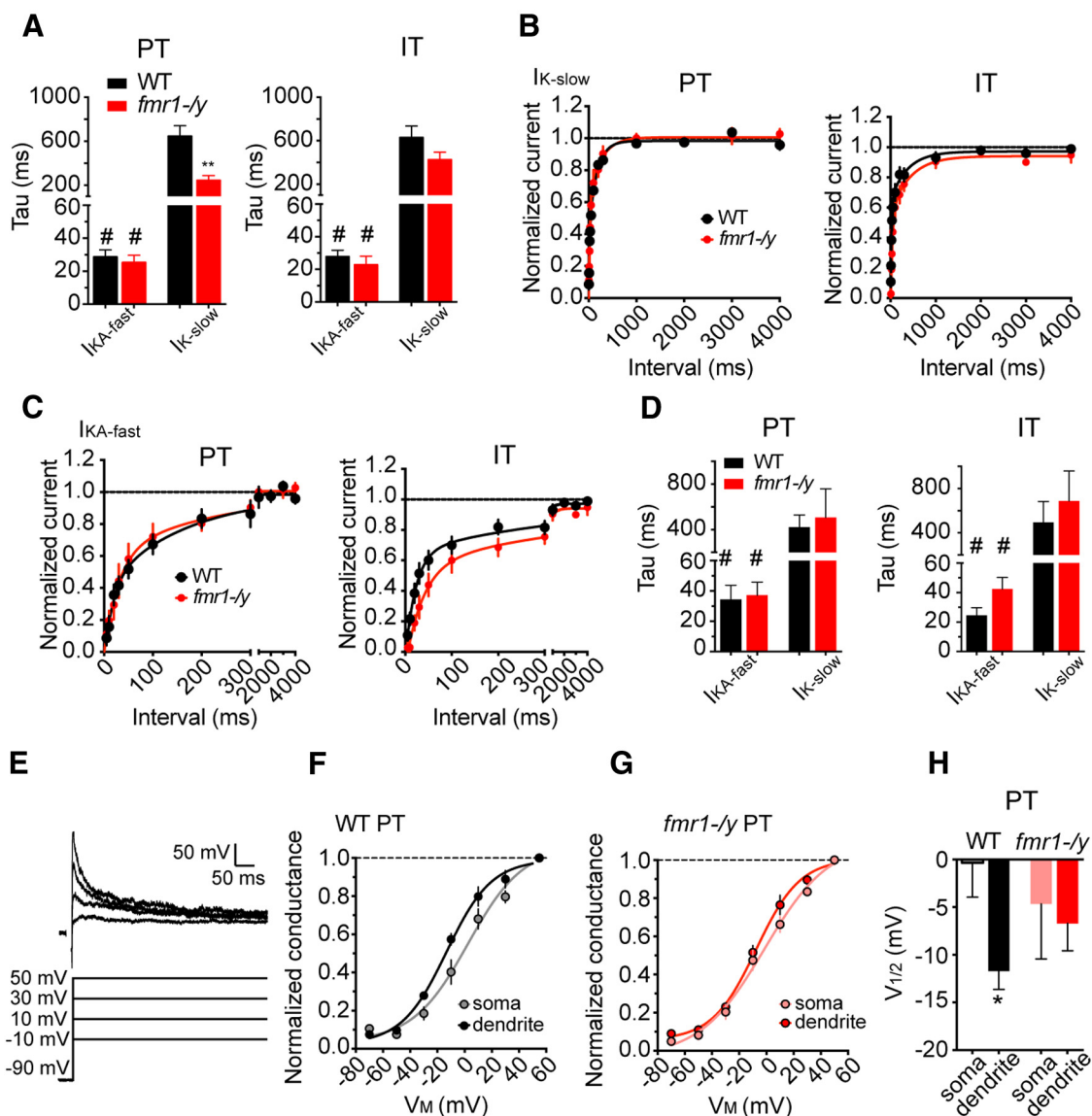


**Figure 8. Kinetic properties of  $K^+$  channels in L5 neurons of PFC.** **A**, The time constant of inactivation of  $I_{K-slow}$  is significantly longer than  $I_{K-fast}$  in both PT (left) and IT (right) neurons.  $\#p < 0.05$ . Additionally, in PT neurons, the time constant of inactivation of  $I_{K-slow}$  was shorter in *fmr1-ly* neurons compared with WT.  $*p < 0.01$ . **B**, Amount of  $I_{K-slow}$  recovered from inactivation, normalized to maximum current, in PT (left) and (right) IT neurons. **C**, Amount of  $I_{K-fast}$  recovered from inactivation, normalized to maximum current, in PT (left) and IT neurons (right). **D**, Time constant for recovery from inactivation data plotted in **B** and **C** for PT (left) and IT (right) neurons.  $\#p < 0.05$  *post hoc* comparison between current types in same genotype. **E**, Protocol for measuring voltage dependence of  $I_{KA}$ . **F**, In WT neurons, the steady-state activation curve is shifted to hyperpolarized potentials in the dendrite relative to the soma. **G**, In contrast, there is no difference in the activation curves between the soma and dendrite in *fmr1-ly* neurons. **H**, the  $V_{1/2}$  of activation is hyperpolarized in the dendrite compared with the soma in WT neurons. In contrast, there is no difference in the  $V_{1/2}$  of activation between the soma and dendrite in *fmr1-ly* neurons.

adjusted to be just-threshold for the generation of an action potential (Fig. 10A). Action potential threshold varied as a function of current duration in both genotypes ( $p < 0.001$ , ANOVA<sup>q</sup>). However, for durations greater than 6 ms, spike threshold was significantly more hyperpolarized in *fmr1-ly* PT neurons compared with WT neurons ( $p < 0.01$ ; *post hoc* comparisons<sup>h</sup>; Fig. 10A–C). Furthermore, the current required to generate an action potential was significantly lower in *fmr1-ly* compared with WT neurons at all current durations ( $p < 0.001$ , ANOVA<sup>i</sup>). Differences

in  $Na^+$  channel availability can produce differences in action potential threshold (Hodgkin and Huxley, 1952). However, there was no significant difference in the maximum rate of rise of action potentials in WT versus *fmr1-ly* neurons, a spike parameter sensitive to  $Na^+$  channel availability ( $p = 0.30$ ; ANOVA<sup>i</sup>; Colbert et al., 1997). There was also no difference in action potential amplitude between genotypes ( $p = 0.59$ ; ANOVA). Finally, there were no differences in action potential threshold between WT and *fmr1-ly* IT neurons ( $p = 0.31$ ; ANOVA; Fig. 10D<sup>k</sup>).

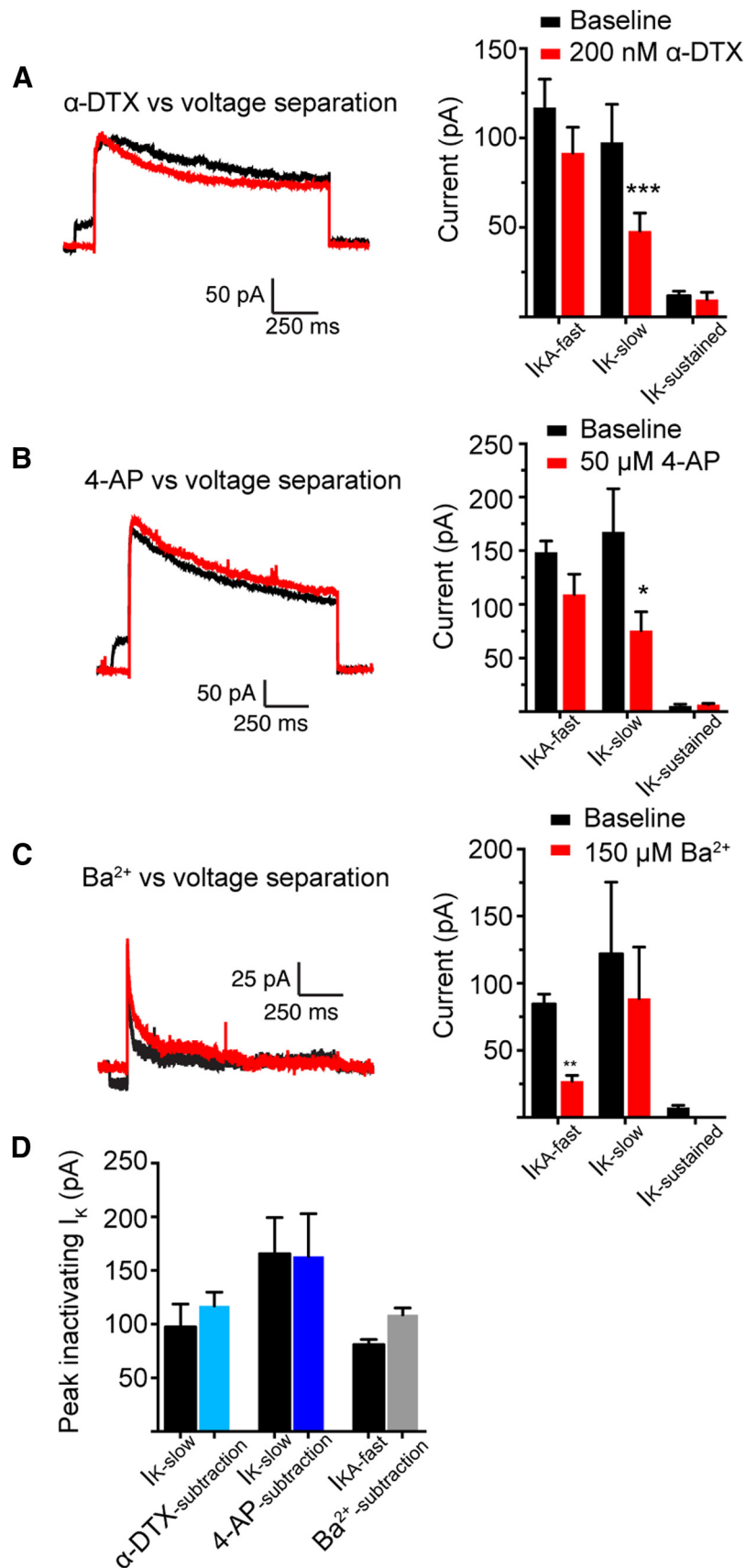


Figure 9. **Sensitivity of  $K^+$  currents to  $K^+$  channel blockers.** **A**, Sample sweeps recorded from the same patch comparing the  $\alpha$ -DTX-sensitive current to  $I_{K-slow}$ .  $\alpha$ -DTX (200 nM) affected  $I_{K-slow}$ , but not other  $K^+$  currents. **B**, Sample sweeps comparing the

continued

4-AP-sensitive current to  $I_{K\text{-slow}}$ . 4-AP (50  $\mu\text{M}$ ) affected  $I_{K\text{-slow}}$ , but not other  $\text{K}^+$  currents. **C**, Sample sweeps comparing the  $\text{Ba}^{2+}$ -sensitive current to  $I_{K\text{A-fast}}$ .  $\text{Ba}^{2+}$  (150  $\mu\text{M}$ ) affected  $I_{K\text{-slow}}$ , but not other  $\text{K}^+$  currents. **D**, Summary of currents obtained via voltage separation versus  $\text{K}^+$  channel blockers. The amplitude of 4-AP and  $\alpha$ -DTX-sensitive current is similar to the amplitude of  $I_{K\text{-slow}}$  obtained via voltage separation, whereas the amplitude of the  $\text{Ba}^{2+}$ -sensitive current is similar to  $I_{K\text{A-fast}}$ .

Together with our outside-out patch recordings, these data suggest that differences in  $\text{K}^+$  channel expression in PT, but not IT neurons, contribute to alterations in spike threshold dynamics in the *fmr1*-/*ly* mouse mPFC, resulting in an increase in excitability.

As an additional test that differences in  $\text{K}^+$  channel function contribute to differences in excitability, we measured the sensitivity of threshold to 50  $\mu\text{M}$  4-AP and 150  $\mu\text{M}$   $\text{Ba}^{2+}$ , and 200 nM  $\alpha$ -DTX. Bath application of 50  $\mu\text{M}$  4-AP produced a decrease in threshold for all but the shortest current durations in both genotypes (WT and *fmr1*-/*ly*;  $n = 6$  cells from 4 mice;  $p < 0.01$ , ANOVA<sup>l</sup>). This effect, however, was larger in WT compared with *fmr1*-/*ly* neurons, consistent with a lower contribution of  $\text{K}_v1$ -containing channels and in agreement with our current measurements ( $p < 0.01$ ; Fig. 11A<sup>m</sup>). Similarly, 200 nM  $\alpha$ -DTX produced a larger affect on threshold in WT compared with *fmr1*-/*ly* neurons (WT and *fmr1*-/*ly*;  $n = 5$  cells from 4 mice;  $p = 0.02$ ; ANOVA; Fig. 11B<sup>n</sup>).  $\text{Ba}^{2+}$  (150  $\mu\text{M}$ ) produced a small but significant decrease in threshold for all but the shortest current durations in both genotypes (WT and *fmr1*-/*ly*;  $n = 8$  from 4 and 5 mice, respectively;  $p < 0.01$ ; ANOVA; Fig. 11C<sup>o</sup>). Interestingly, in WT mice the effect of 4-AP and  $\alpha$ -DTX was larger than that of  $\text{Ba}^{2+}$  ( $p < 0.001$ , ANOVA<sup>p</sup>), whereas in *fmr1*-/*ly* mice there was no difference in the effect of these  $\text{K}^+$  channel blockers ( $p = 0.55$ , ANOVA; Fig. 11D<sup>q</sup>). These data suggest that in *fmr1*-/*ly* PT neurons, a decrease in  $\text{K}_v1$ -mediated  $\text{K}^+$  current contributes to an increase in excitability.

## Discussion

We have provided evidence for neuron-type-specific channelopathies within a single brain region in FXS. We observed several differences in the functional expression of ion channels in L5 neurons of mPFC in the *fmr1*-/*ly* mouse (Fig. 12). At the soma and dendrite, we observed differences in the subthreshold properties of *fmr1*-/*ly* PT neurons consistent with a decrease in  $I_h$  compared with WT neurons. These differences were largely eliminated by the application of the h-channel blocker ZD7288, suggesting that they were mediated, in part, by differences in h-channels. Consistent with this, we observed less  $I_h$  at the distal dendrite of *fmr1*-/*ly* PT neurons, suggesting that there is a reduction in functional h-channels. Additionally, we found alterations to several  $\text{K}^+$  channels at the soma of PT neurons. Compared with WT neurons, *fmr1*-/*ly* neurons possessed greater maximum fast-inactivating A-type  $\text{K}^+$  current, but less slow-inactivating  $\text{K}^+$  current. The kinetics and pharmacologic sensitivity of these currents was consistent with  $\text{K}_v4$  and  $\text{K}_v1$  containing channels, respectively. In contrast to PT neurons, there were no genotypic differences in the maximum amplitude of these  $\text{K}^+$  currents at the soma of IT neurons. As a functional

consequence of altered somatic  $\text{K}^+$  channel function in PT neurons, we observed an increase in excitability.

These findings expand on previous reports of channelopathies in various brain regions by demonstrating neuron specific phenotypes within a brain region (Brager and Johnston, 2014). In L5B neurons of somatosensory cortex a decrease in h-channel expression, together with altered BK channel function, contributes to a lowered threshold for dendritic  $\text{Ca}^{2+}$  electrogenesis (Zhang et al., 2014). In contrast to somatosensory cortex, there is an increase in h-channel expression in CA1 pyramidal neurons in the *fmr1*-/*ly* mouse (Brager et al., 2012). Additionally, in CA1 pyramidal neurons, there is a decrease in  $\text{K}_v4$ -mediated A-type  $\text{K}^+$  current (Routh et al., 2013). Our data, together with these previously published findings, suggest that in FXS the function of a given ion channel can be affected in opposite ways depending upon brain region. More importantly, the absence of differences in  $\text{K}^+$  channel function in IT neurons suggests that neuron-specific channel phenotypes can occur even within a brain region, between different classes of principal neurons (Fig. 12). Alterations to other channel types reported in various brain regions may similarly display neuron-type specificity.

### Identity of $\text{K}^+$ channels altered in mPFC

$\text{K}_v1$  and  $\text{K}_v4$  containing channels contribute to transient  $\text{K}^+$  currents (Coetzee et al., 1999). Although the details depend upon which auxiliary subunits are present,  $\text{K}_v4$  channels inactivate and recover from inactivation an order of a magnitude faster than  $\text{K}_v1$  channels (Castellino et al., 1995; An et al., 2000; Jerng et al., 2004; Kim et al., 2008). Thus, the  $I_{K\text{A-fast}}$  we observed is consistent with  $\text{K}_v4$  containing channels whereas the  $I_{K\text{-slow}}$  is consistent with  $\text{K}_v1$  channels. Several subunits within the  $\text{K}_v1$  and  $\text{K}_v4$  families can contribute to transient  $\text{K}^+$  currents (Coetzee et al., 1999). There is evidence that  $\text{K}_v4.2$ ,  $4.3$ , and  $1.4$  contribute to transient  $\text{K}^+$  currents at the soma of cortical pyramidal neurons (Carrasquillo et al., 2012). In addition,  $\text{K}_v1.2$  containing channels contribute to a slowly inactivating  $\text{K}^+$  current at the soma (Bekkers and Delaney, 2001). All of these subunits have been reported to contribute to action potential threshold and thus alterations to any of these subunits could contribute to differences in  $I_K$  and excitability we observe (Bekkers and Delaney, 2001; Kim et al., 2005; Kole et al., 2007; Higgs and Spain, 2011). Regardless of the subunit, the differences in maximum current we observed are consistent with a decrease in the number of  $\text{K}_v1$  channels and an increase in  $\text{K}_v4$  channels in PT neurons of mPFC in the *fmr1*-/*ly* mouse.

### Potential mechanisms

Brain region-specific channel phenotypes in FXS could be caused by a primary deficiency in an FMRP-mediated

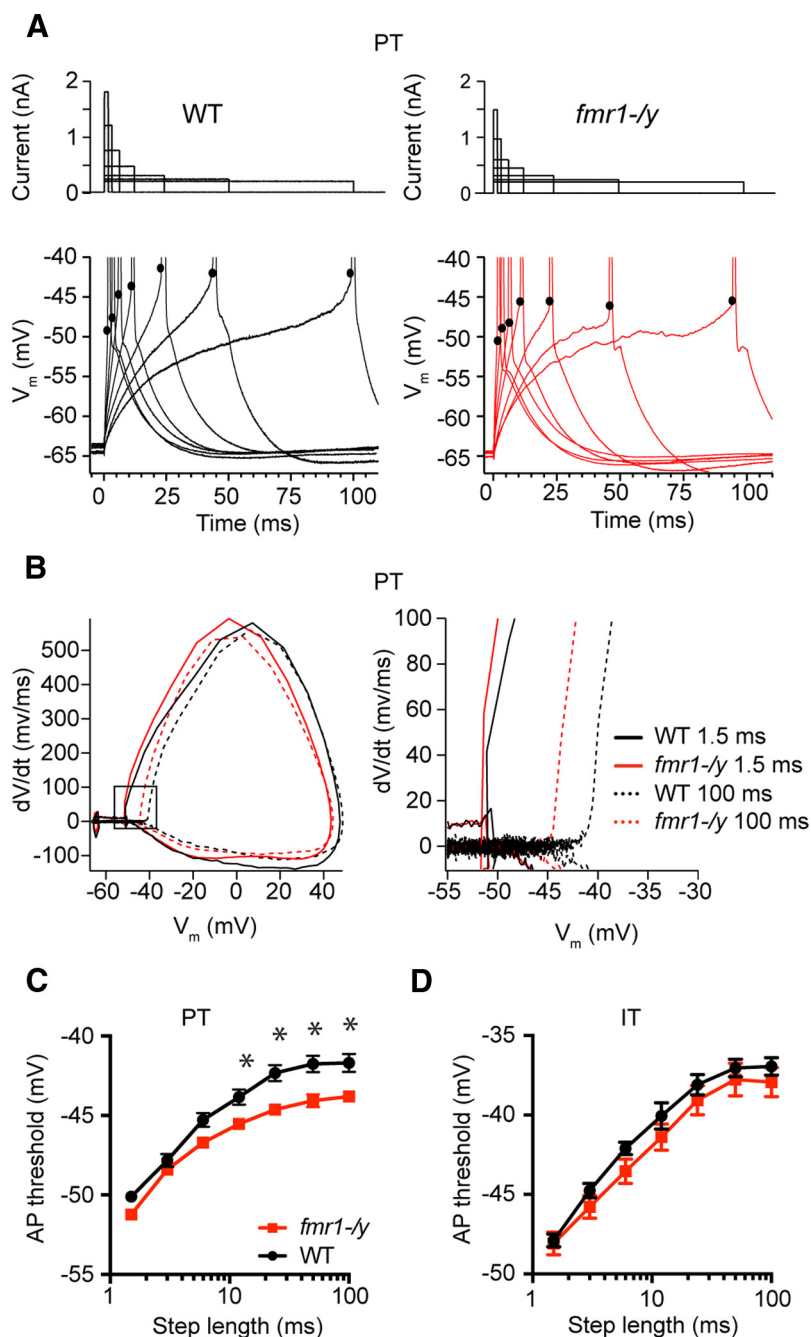
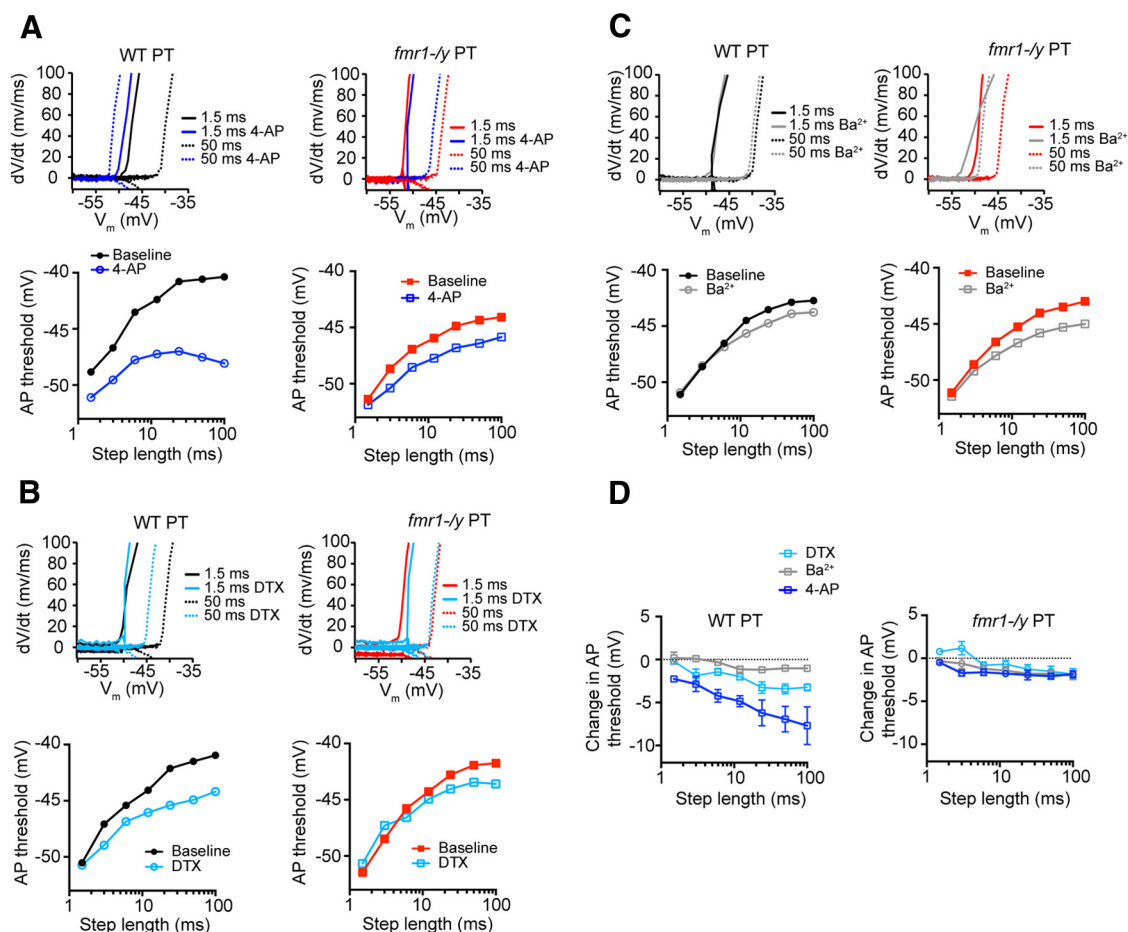


Figure 10. ***Fmr1-ly* PT neurons are more excitable compared with WT neurons.** **A**, The threshold for action potential generation in WT and *fmr1-ly* neurons was measured in response to just threshold current injections of increasing duration. Sample action potentials for each genotype are shown below. **B**, Phase plane plot of action potentials in *fmr1-ly* and WT PT neurons in response to 1.5 and 100 ms current injection. **C**, *fmr1-ly* neurons displayed a lower threshold for action potential generation for all current injections longer than 6 ms. **D**, There were no differences in threshold between *fmr1-ly* and WT IT neurons. \* $p < 0.01$  comparison between genotypes.

process within the cell. FMRP is an mRNA binding protein and has been shown to negatively regulate protein synthesis through ribosomal stalling (Li et al., 2001; Zalfa et al., 2003; Darnell et al., 2011). Consequently, the absence of FMRP could lead to elevated expression of ion channel proteins and/or their regulatory subunits. More recent evidence suggests that FMRP can also promote

the translation of certain mRNAs (Bechara et al., 2009; Fählng et al., 2009; Gross et al., 2011). Thus, the absence of FMRP might then reduce the expression of ion channel proteins. In addition to its role in translation, FMRP participates in the activity-dependent transport of mRNA granules from the soma to axonal and dendritic locations (Antar et al., 2004; Kanai et al., 2004; Dichtenberg et al.,



**Figure 11. *Fmr1-ly* neurons are less sensitive to Kv1 channel blockers compared with WT neurons.** **A**, Phase plane plots for action potentials generated in response to 1.5 and 50 ms current injections before and after 50  $\mu\text{M}$  4-AP application. 4-AP decreased threshold in both genotypes, but more so in WT neurons. **B**, Phase plane plots for action potentials generated before and after 200 nM  $\alpha$ -DTX application.  $\alpha$ -DTX decreased threshold in both genotypes, but more so in WT neurons. **C**, Phase plane plots for action potentials generated before and after 150  $\mu\text{M}$   $\text{Ba}^{2+}$  application.  $\text{Ba}^{2+}$  decreased action potential threshold in both genotypes. **D**, 4-AP and  $\alpha$ -DTX application had a larger effect on action potential threshold compared with  $\text{Ba}^{2+}$  in WT neurons. In contrast, 4-AP and  $\alpha$ -DTX had the same effect on action potential threshold compared with  $\text{Ba}^{2+}$  in *fmr1-ly* neurons. For current steps longer than 6 ms, there was significant difference in the effect of 4-AP and/or  $\alpha$ -DTX on threshold between WT and *fmr1-ly* mice.

2008). The absence of FMRP could therefore result in the trapping of ion channel mRNAs at the soma or the mislocalization of mRNAs and the encoded proteins. Both h-channel and A-type  $\text{K}^+$  channel mRNAs are known targets of FMRP (Gross et al., 2011; Lee et al., 2011; Darnell et al., 2011). Therefore, the channel phenotypes observed in FXS could be because of either of these mRNA regulatory processes. Lastly, FMRP can directly bind to target proteins, including ion channel subunits. Consequently, the absence of FMRP could alter the biophysical properties or surface expression of ion channels by promoting inappropriate subunit assemblies (Brown et al., 2010; Deng et al., 2013). It is noteworthy that in order to sufficiently explain the divergent channel phenotype we observe, these cellular processes would have to promote or suppress the function of a given ion channel in a neuron-specific manner.

Alternatively, the differences in channel function we observe could be the result of secondary changes in

response to altered processes extrinsic to the cell. Both  $I_h$  and  $I_{KA}$  undergo synaptic-driven changes (Frick et al., 2004; Fan et al., 2005; Brager and Johnston, 2007; Losonczy et al., 2008). Thus, a potential cell extrinsic mechanism could involve changes in synaptic input to mPFC neurons that result in changes in ion channel function opposite to those that occur in CA1. Indeed there is evidence that synaptic input to neocortical and hippocampal pyramidal neurons is altered in the *fmr1-ly* mouse (Bureau et al., 2008; Gibson et al., 2008; Hays et al., 2011; Krueger et al., 2011; Testa-Silva et al., 2012; Patel et al., 2013; Tyzio et al., 2014). In addition, the function of both  $I_h$  and  $I_{KA}$  are affected by neuromodulation (Hoffman and Johnston, 1999; Carr et al., 2007; Dembrow et al., 2010). Thus, the divergent channel phenotypes observed in CA1 and neocortex could be caused by differences in neuromodulation. Determining whether neuron-type-specific alterations to ion channel function are caused by a cell autonomous or cell extrinsic mech-

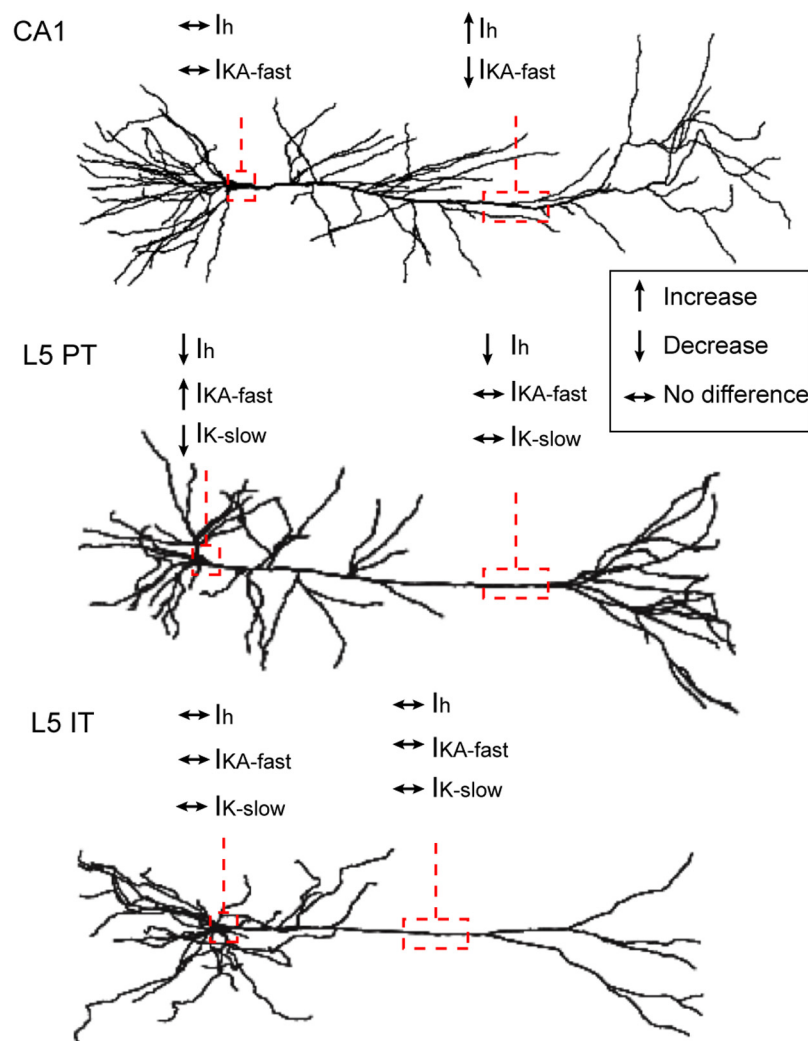


Figure 12. **Summary of neuron type-specific channel phenotypes observed in the *fmr1*<sup>-/-</sup> mouse.** Dendritic and somatic  $I_h$ ,  $I_{KA}$ -fast, and  $I_K$ -slow levels in the *fmr1*<sup>-/-</sup> mouse relative to WT in CA1 pyramidal neurons (Brager et al., 2012; Routh et al., 2013), L5 PT neurons of PFC and IT neurons of PFC. There is also a decrease in  $I_h$  in the dendrites of L5 neurons of somatosensory cortex (data not shown; Zhang et al, 2014). Upward arrow indicates increase relative to WT. Downward arrow indicates decrease relative to WT. Horizontal arrow indicates no difference relative to WT.

anism (eg, differences in network activity) is a difficult challenge, yet fundamental to our understanding of the neurobiology of FXS.

### Functional implications

The combined effects of the channel phenotypes we observe could have a substantial impact on mPFC function. PT neurons receive synaptic input in L1 from various sources and the presence of  $I_h$  greatly influences the transfer of these inputs to the soma (Dembrow et al., 2015). Specifically,  $I_h$  contributes to the filtering properties of the membrane such that inputs arriving in the theta frequency range are selectively transferred to the soma (Ulrich, 2002; Cook et al., 2007). Additionally,  $I_h$  compensates for distance dependent temporal delays imposed by the dendrite, ensuring that distal inputs arrive at the soma with a similar latency to proximal ones (Vaidya and Johnston, 2013). This has the effect of narrowing the temporal

window under which synaptic input arriving at different dendritic locations can summate at the soma to drive an action potential (Dembrow et al., 2015). Thus, the decrease in  $I_h$  we observe in the *fmr1*<sup>-/-</sup> mouse could: (1) affect the frequency preference of PT neurons to synaptic input, and (2) increase integration at the soma of asynchronous dendritic synaptic inputs. Consequently, *fmr1*<sup>-/-</sup> PT neurons may function as temporal integrators of synaptic input, in contrast with WT PT neurons, which function as coincidence detectors (Dembrow et al., 2015).

These changes in  $I_h$  could work synergistically with  $K^+$  channel alterations to make *fmr1*<sup>-/-</sup> PT neurons generally more responsive to synaptic input.  $K^+$  channels affect the threshold for spike generation in part by influencing the voltage at the axon initiation site (Bekkers and Delaney, 2001; Kole et al., 2007). Like h-channels,  $K^+$  channels contribute to the band pass filtering properties of the membrane. Thus, the changes in  $K^+$  channels we observe

could also decrease the preference of PT neurons for high-frequency input as has been observed upon blockade of Kv1 channels in L2/3 neurons (Higgs and Spain, 2011). Together with changes to synaptic input, these changes may contribute to altered up-states observed in cortical pyramidal neurons in the *fmr1-/-* mouse (Hays et al., 2011; Gonçalves et al., 2013).

FXS patients display behavioral deficits associated with PFC dysfunction, including hyperactivity, attention deficits, impulsivity, and behavioral inflexibility. The channel phenotypes we describe here may thus contribute to these behavioral phenotypes. Finally, our findings of cell-type-specific phenotypes highlights the challenges associated with developing effective treatment strategies in FXS. A critical implication of our findings is that existing therapies that target a given channel phenotype, although effective in treating one feature of FXS could simultaneously exacerbate others. Understanding the mechanisms of these neuron/brain region-specific effects in FXS may prove critical in developing treatment strategies.

## References

- An WF, Bowlby MR, Betty M, Cao J, Ling HP, Mendoza G, Hinson JW, Mattsson KI, Strassle BW, Trimmer JS, Rhodes KJ (2000) Modulation of A-type potassium channels by a family of calcium sensors. *Nature* 403:553–556. [CrossRef](#) [Medline](#)
- Antar LN, Afroz R, Dichtenberg JB, Carroll RC, Bassell GJ (2004) Metabotropic glutamate receptor activation regulates fragile x mental retardation protein and FMR1 mRNA localization differentially in dendrites and at synapses. *J Neurosci* 24:2648–2655. [CrossRef](#) [Medline](#)
- Avesar D, Gullledge AT (2012) Selective serotonergic excitation of callosal projection neurons. *Front Neural Circuits* 6. [CrossRef](#) [Medline](#)
- Bechara EG, Didiot MC, Melko M, Davidovic L, Bensaid M, Martin P, Castets M, Pognonec P, Khandjian EW, Moine H, Bardoni B (2009) A novel function for fragile X mental retardation protein in translational activation. *PLoS Biol* 7:e16 [CrossRef](#) [Medline](#)
- Bekkers JM (2000) Distribution and activation of voltage-gated potassium channels in cell-attached and outside-out patches from large layer 5 cortical pyramidal neurons of the rat. *J Physiol* 525:611–620. [Medline](#)
- Bekkers JM, Delaney AJ (2001) Modulation of excitability by alpha-dendrotoxin-sensitive potassium channels in neocortical pyramidal neurons. *J Neurosci* 21:6553–6560. [Medline](#)
- Bernard C, Anderson A, Becker A, Poolos NP, Beck H, Johnston D (2004) Acquired dendritic channelopathy in temporal lobe epilepsy. *Science* 305:532–535. [CrossRef](#) [Medline](#)
- Bhakar AL, Dölen G, Bear MF (2012) The pathophysiology of fragile X (and what it teaches us about synapses). *Annu Rev Neurosci* 35:417–443. [CrossRef](#) [Medline](#)
- Brager DH, Akhavan AR, Johnston D (2012) Impaired dendritic expression and plasticity of h-channels in the *fmr1(-/-)* mouse model of fragile X syndrome. *Cell Rep* 1:225–233. [CrossRef](#) [Medline](#)
- Brager DH, Johnston D (2007) Plasticity of intrinsic excitability during long-term depression is mediated through mGluR-dependent changes in  $I_h$  in hippocampal CA1 pyramidal neurons. *J Neurosci* 27:13926–13937. [CrossRef](#) [Medline](#)
- Brager DH, Johnston D (2014) Channelopathies and dendritic dysfunction in fragile X syndrome. *Brain Res Bull* 103:11–17. [CrossRef](#) [Medline](#)
- Brown MR, Kronengold J, Gazula V-R, Chen Y, Strumbos JG, Sigworth FJ, Navaratnam D, Kaczmarek LK (2010) Fragile X mental retardation protein controls gating of the sodium-activated potassium channel Slack. *Nat Neurosci* 13:819–821. [CrossRef](#) [Medline](#)
- Bureau I, Shepherd GMG, Svoboda K (2008) Circuit and plasticity defects in the developing somatosensory cortex of *Fmr1* knock-out mice. *J Neurosci* 28:5178–5188. [CrossRef](#)
- Carr DB, Andrews GD, Glen WB, Lavin A (2007) 2-Noradrenergic receptors activation enhances excitability and synaptic integration in rat prefrontal cortex pyramidal neurons via inhibition of HCN currents. *J Physiol* 584:437–450. [CrossRef](#) [Medline](#)
- Carrasquillo Y, Burkhalter A, Nerbonne JM (2012) A-type K<sup>+</sup> channels encoded by Kv4.2, Kv4.3, and Kv1.4 differentially regulate intrinsic excitability of cortical pyramidal neurons. *J Physiol* 590:3877–3890. [CrossRef](#) [Medline](#)
- Castellino RC, Morales MJ, Strauss HC, Rasmuson RL (1995) Time- and voltage-dependent modulation of a Kv1.4 channel by a beta-subunit (Kv beta 3) cloned from ferret ventricle. *Am J Physiol* 269:H385–H391. [Medline](#)
- Castle NA, Fadous S, Logothetis DE, Wang GK (1994) Aminopyridine block of Kv1.1 potassium channels expressed in mammalian cells and *Xenopus* oocytes. *Mol Pharmacol* 45:1242–1252. [Medline](#)
- Christophe E, Doerflinger N, Lavery DJ, Molnár Z, Charpak S, Audinat E (2005) Two populations of layer V pyramidal cells of the mouse neocortex: development and sensitivity to anesthetics. *J Neurophysiol* 94:3357–3367. [CrossRef](#) [Medline](#)
- Coetzee WA, Amarillo Y, Chiu J, Chow A, Lau D, McCormack T, Moreno H, Nadal MS, Ozaita A, Pountney D, Saganich M, Vega-Saenz de Miera E, Rudy B (1999) Molecular diversity of K<sup>+</sup> channels. *Ann N Y Acad Sci* 868:233–285. [Medline](#)
- Colbert CM, Magee JC, Hoffman DA, Johnston D (1997) Slow recovery from inactivation of Na<sup>+</sup> channels underlies the activity-dependent attenuation of dendritic action potentials in hippocampal CA1 pyramidal neurons. *J Neurosci* 17:6512–6521. [Medline](#)
- Contractor A, Klyachko VA, Portera-Cailliau C (2015) Altered neuronal and circuit excitability in fragile X syndrome. *Neuron* 87:699–715. [CrossRef](#) [Medline](#)
- Cook EP, Guest JA, Liang Y, Masse NY, Colbert CM (2007) Dendrite-to-soma input/output function of continuous time-varying signals in hippocampal CA1 pyramidal neurons. *J Neurophysiol* 98:2943–2955. [CrossRef](#) [Medline](#)
- Darnell JC, Van Driesche SJ, Zhang C, Hung KYS, Mele A, Fraser CE, Stone EF, Chen C, Fak JJ, Chi SW, Licatalosi DD, Richter JD, Darnell RB (2011) FMRP stalls ribosomal translocation on mRNAs linked to synaptic function and autism. *Cell* 146:247–261. [CrossRef](#) [Medline](#)
- Dembrow N, Johnston D (2014) Subcircuit-specific neuromodulation in the prefrontal cortex. *Front Neural Circuits* 8:54. [CrossRef](#) [Medline](#)
- Dembrow NC, Chitwood RA, Johnston D (2010) Projection-specific neuromodulation of medial prefrontal cortex neurons. *J Neurosci* 30:16922–16937. [CrossRef](#) [Medline](#)
- Dembrow NC, Zemelman BV, Johnston D (2015) Temporal dynamics of L5 dendrites in medial prefrontal cortex regulate integration versus coincidence detection of afferent inputs. *J Neurosci* 35:4501–4514. [CrossRef](#) [Medline](#)
- Deng P-Y, Rotman Z, Blundon JA, Cho Y, Cui J, Cavalli V, Zakharenko SS, Klyachko VA (2013) FMRP regulates neurotransmitter release and synaptic information transmission by modulating action potential duration via BK channels. *Neuron* 77:696–711. [CrossRef](#)
- Dichtenberg JB, Swanger SA, Antar LN, Singer RH, Bassell GJ (2008) A direct role for FMRP in activity-dependent dendritic mRNA transport links filopodial-spine morphogenesis to fragile X syndrome. *Developmental Cell* 14:926–939. [CrossRef](#) [Medline](#)
- Dougherty KA, Nicholson DA, Diaz L, Buss EW, Neuman KM, Chetkovich DM, Johnston D (2013) Differential expression of HCN subunits alters voltage-dependent gating of h-channels in CA1 pyramidal neurons from dorsal and ventral hippocampus. *J Neurophysiol* 109:1940–1953. [CrossRef](#) [Medline](#)
- Fähling M, Mrowka R, Steege A, Kirschner KM, Benko E, Förster B, Persson PB, Thiele BJ, Meier JC, Scholz H (2009) Translational regulation of the human Achaete-scute homologue-1 by fragile X

- mental retardation protein. *Journal of Biological Chemistry* 284:4255–4266. [CrossRef Medline](#)
- Fan Y, Fricker D, Brager DH, Chen X, Lu H-C, Chitwood RA, Johnston D (2005) Activity-dependent decrease of excitability in rat hippocampal neurons through increases in *I<sub>h</sub>*. *Nat Neurosci* 8:1542–1551. [CrossRef](#)
- Frick A, Magee J, Johnston D (2004) LTP is accompanied by an enhanced local excitability of pyramidal neuron dendrites. *Nat Neurosci* 7:126–135. [CrossRef Medline](#)
- Gasparini S, Losonczy A, Chen X, Johnston D, Magee JC (2007) Associative pairing enhances action potential back-propagation in radial oblique branches of CA1 pyramidal neurons. *J Physiol* 580:787–800. [CrossRef Medline](#)
- Gee S, Ellwood I, Patel T, Luongo F, Deisseroth K, Sohal VS (2012) Synaptic activity unmasks dopamine D2 receptor modulation of a specific class of layer V pyramidal neurons in prefrontal cortex. *J Neurosci* 32:4959–4971. [CrossRef Medline](#)
- Gibson JR, Bartley AF, Hays SA, Huber KM (2008) Imbalance of neocortical excitation and inhibition and altered UP states reflect network hyperexcitability in the mouse model of fragile X syndrome. *J Neurophysiol* 100:2615–2626. [CrossRef Medline](#)
- Gonçalves JT, Anstey JE, Golshani P, Portera-Cailliau C (2013) Circuit level defects in the developing neocortex of fragile X mice. *Nat Neurosci* 16:903–909. [CrossRef Medline](#)
- Gross C, Yao X, Pong DL, Jeromin A, Bassell GJ (2011) Fragile X mental retardation protein regulates protein expression and mRNA translation of the potassium channel Kv4.2. *J Neurosci* 31:5693–5698. [CrossRef Medline](#)
- Hagerman RJ, Ono MY, Hagerman PJ (2005) Recent advances in fragile X: a model for autism and neurodegeneration. *Curr Opin Psychiatry* 18:490–496. [CrossRef Medline](#)
- Harris-Warrick RM, Coniglio LM, Levini RM, Gueron S, Guckenheimer J (1995) Dopamine modulation of two subthreshold currents produces phase shifts in activity of an identified motoneuron. *J Neurophysiol* 74:1404–1420. [Medline](#)
- Harvey AL (2001) Twenty years of dendrotoxins. *Toxicol* 39:15–26. [Medline](#)
- Hattox AM, Nelson SB (2007) Layer V neurons in mouse cortex projecting to different targets have distinct physiological properties. *J Neurophysiol* 98:3330–3340. [CrossRef Medline](#)
- Hays SA, Huber KM, Gibson JR (2011) Altered neocortical rhythmic activity states in *Fmr1* KO mice are due to enhanced mGluR5 signaling and involve changes in excitatory circuitry. *J Neurosci* 31:14223–14234. [CrossRef Medline](#)
- Higgs MH, Spain WJ (2011) Kv1 channels control spike threshold dynamics and spike timing in cortical pyramidal neurones. *J Physiol* 589:5125–5142. [CrossRef Medline](#)
- Hodgkin AL, Huxley AF (1952) A quantitative description of membrane current and its application to conduction and excitation in nerve. *J Physiol* 117:500–544. [Medline](#)
- Hoffman DA, Johnston D (1999) Neuromodulation of dendritic action potentials. *J Neurophysiol* 81:408–411. [Medline](#)
- Hutcheon B, Yarom Y (2000) Resonance, oscillation and the intrinsic frequency preferences of neurons. *Trends Neurosci* 23:216–222. [Medline](#)
- Jerng HH, Pfaffinger PJ, Covarrubias M (2004) Molecular physiology and modulation of somatodendritic A-type potassium channels. *Mol Cell Neurosci* 27:343–369. [CrossRef Medline](#)
- Johnston D, Narayanan R (2008) Active dendrites: colorful wings of the mysterious butterflies. *Trends Neurosci* 31:309–316. [CrossRef Medline](#)
- Kalmbach BE, Chitwood RA, Dembrow NC, Johnston D (2013) Dendritic generation of mGluR-mediated slow afterdepolarization in layer 5 neurons of prefrontal cortex. *J Neurosci* 33:13518–13532. [CrossRef Medline](#)
- Kanai Y, Dohmae N, Hirokawa N (2004) Kinesin Transports RNA. *Neuron* 43:513–525. [CrossRef Medline](#)
- Kim J, Nadal MS, Clemens AM, Baron M, Jung S-C, Misumi Y, Rudy B, Hoffman DA (2008) Kv4 accessory protein DPPX (DPP6) is a critical regulator of membrane excitability in hippocampal CA1 pyramidal neurons. *J Neurophysiol* 100:1835–1847. [CrossRef Medline](#)
- Kim J, Wei DS, Hoffman DA (2005) Kv4 potassium channel subunits control action potential repolarization and frequency-dependent broadening in rat hippocampal CA1 pyramidal neurones. *J Physiol* 569:41–57. [CrossRef Medline](#)
- Kole MHP, Hallermann S, Stuart GJ (2006) Single *I<sub>h</sub>* channels in pyramidal neuron dendrites: properties, distribution, and impact on action potential output. *J Neurosci* 26:1677–1687. [CrossRef Medline](#)
- Kole MHP, Letzkus JJ, Stuart GJ (2007) Axon initial segment Kv1 channels control axonal action potential waveform and synaptic efficacy. *Neuron* 55:633–647. [CrossRef Medline](#)
- Korngreen A, Sakmann B (2000) Voltage-gated K<sup>+</sup> channels in layer 5 neocortical pyramidal neurones from young rats: subtypes and gradients. *J Physiol* 525 Pt 3:621–639. [Medline](#)
- Krueger DD, Osterweil EK, Chen SP, Tye LD, Bear MF (2011) Cognitive dysfunction and prefrontal synaptic abnormalities in a mouse model of fragile X syndrome. *Proc Natl Acad Sci* 108:2587–2592. [CrossRef Medline](#)
- Lee AT, Gee SM, Vogt D, Patel T, Rubenstein JL, Sohal VS (2014) Pyramidal neurons in prefrontal cortex receive subtype-specific forms of excitation and inhibition. *Neuron* 81:61–68. [CrossRef Medline](#)
- Lee HY, Ge W-P, Huang W, He Y, Wang GX, Rowson-Baldwin A, Smith SJ, Jan YN, Jan LY (2011) Bidirectional regulation of dendritic voltage-gated potassium channels by the fragile X mental retardation protein. *Neuron* 72:630–642. [CrossRef Medline](#)
- Li Z, Zhang Y, Ku L, Wilkinson KD, Warren ST, Feng Y (2001) The fragile X mental retardation protein inhibits translation via interacting with mRNA. *Nucleic Acids Res* 29:2276–2283. [Medline](#)
- London M, Häusser M (2005) Dendritic Computation. *Annu Rev Neurosci* 28:503–532. [CrossRef Medline](#)
- Losonczy A, Makara JK, Magee JC (2008) Compartmentalized dendritic plasticity and input feature storage in neurons. *Nature* 452:436–441. [CrossRef Medline](#)
- Lörincz A, Notomi T, Tamás G, Shigemoto R, Nusser Z (2002) Polarized and compartment-dependent distribution of HCN1 in pyramidal cell dendrites. *Nat Neurosci* 5:1185–1193. [CrossRef Medline](#)
- Magee JC (2000) Dendritic integration of excitatory synaptic input. *Nat Rev Neurosci* 1:181–190. [CrossRef Medline](#)
- Menon V, Leroux J, White CD, Reiss AL (2004) Frontostriatal deficits in fragile X syndrome: relation to FMR1 gene expression. *Proc Natl Acad Sci* 101:3615–3620. [CrossRef Medline](#)
- Meredith RM, Holmgren CD, Weidum M, Burnashev N, Mansvelder HD (2007) Increased threshold for spike-timing-dependent plasticity is caused by unreliable calcium signaling in mice lacking fragile X gene *Fmr1*. *Neuron* 54:627–638. [CrossRef Medline](#)
- Molnár Z, Cheung AFP (2006) Towards the classification of subpopulations of layer V pyramidal projection neurons. *Neurosci Res* 55:105–115. [CrossRef Medline](#)
- Molyneaux BJ, Arlotta P, Menezes JRL, Macklis JD (2007) Neuronal subtype specification in the cerebral cortex. *Nat Rev Neurosci* 8:427–437. [CrossRef Medline](#)
- Morishima M, Morita K, Kubota Y, Kawaguchi Y (2011) Highly differentiated projection-specific cortical subnetworks. *J Neurosci* 31:10380–10391. [CrossRef Medline](#)
- Narayanan R, Johnston D (2007) Long-Term potentiation in rat hippocampal neurons is accompanied by spatially widespread changes in intrinsic oscillatory dynamics and excitability. *Neuron* 56:1061–1075. [CrossRef Medline](#)
- Otsuka T, Kawaguchi Y (2011) Cell diversity and connection specificity between callosal projection neurons in the frontal cortex. *J Neurosci* 31:3862–3870. [CrossRef Medline](#)
- Patel AB, Hays SA, Bureau I, Huber KM, Gibson JR (2013) A target cell-specific role for presynaptic *Fmr1* in regulating glutamate release onto neocortical fast-spiking inhibitory neurons. *J Neurosci* 33:2593–2604. [CrossRef Medline](#)

- Robinson RB, Siegelbaum SA (2003) Hyperpolarization-activated cation currents: from molecules to physiological function. *Annu Rev Physiol* 65:453–480. [CrossRef](#) [Medline](#)
- Routh BN, Johnston D, Brager DH (2013) Loss of functional A-type potassium channels in the dendrites of CA1 pyramidal neurons from a mouse model of fragile X syndrome. *J Neurosci* 33:19442–19450. [CrossRef](#) [Medline](#)
- Russell SN, Publicover NG, Hart PJ, Carl A, Hume JR, Sanders KM, Horowitz B (1994) Block by 4-aminopyridine of a Kv1.2 delayed rectifier K<sup>+</sup> current expressed in *Xenopus* oocytes. *J Physiol* 481:571–584. [CrossRef](#)
- Santoro MR, Bray SM, Warren ST (2012) Molecular mechanisms of fragile X syndrome: a twenty-year perspective. *Annu Rev Pathol* 7:219–245. [CrossRef](#) [Medline](#)
- Sheets PL, Suter BA, Kiritani T, Chan CS, Surmeier DJ, Shepherd GMG (2011) Corticospinal-specific HCN expression in mouse motor cortex: *I*<sub>h</sub>-dependent synaptic integration as a candidate microcircuit mechanism involved in motor control. *J Neurophysiol* 106:2216–2231. [CrossRef](#)
- Shepherd GMG (2013) Corticostriatal connectivity and its role in disease. *Nat Rev Neurosci* 14:278–291. [CrossRef](#)
- Shin M, Brager D, Jaramillo TC, Johnston D, Chetkovich DM (2008) Mislocalization of h channel subunits underlies h channelopathy in temporal lobe epilepsy. *Neurobiol Dis* 32:26–36. [CrossRef](#) [Medline](#)
- Stephens GJ, Garratt JC, Robertson B, Owen DG (1994) On the mechanism of 4-aminopyridine action on the cloned mouse brain potassium channel mKv1.1. *J Physiol* 477:187–196. [CrossRef](#)
- Strumbos JG, Brown MR, Kronengold J, Polley DB, Kaczmarek LK (2010) Fragile X mental retardation protein is required for rapid experience-dependent regulation of the potassium channel Kv3.1b. *J Neurosci* 30:10263–10271. [CrossRef](#) [Medline](#)
- Testa-Silva G, Loebel A, Giugliano M, de Kock CPJ, Mansvelter HD, Meredith RM (2012) Hyperconnectivity and slow synapses during early development of medial prefrontal cortex in a mouse model for mental retardation and autism. *Cerebral Cortex* 22:1333–1342. [CrossRef](#)
- Tyzio R, Nardou R, Ferrari DC, Tsintsadze T, Shahrokhi A, Eftekhari S, Khalilov I, Tsintsadze V, Brouchoud C, Chazal G, Lemonnier E, Lozovaya N, Burnashev N, Ben-Ari Y (2014) Oxytocin-mediated GABA inhibition during delivery attenuates autism pathogenesis in rodent offspring. *Science* 343:675–679. [CrossRef](#) [Medline](#)
- Ulrich D (2002) Dendritic resonance in rat neocortical pyramidal cells. *J Neurophysiol* 87:2753–2759. [Medline](#)
- Vaidya SP, Johnston D (2013) Temporal synchrony and gamma-to-theta power conversion in the dendrites of CA1 pyramidal neurons. *Nat Neurosci* 16:1812–1820. [CrossRef](#) [Medline](#)
- Wang JM, Koldewyn K, Hashimoto R-I, Schneider A, Le L, Tassone F, Cheung K, Hagerman P, Hessler D, Rivera SM (2012) Male carriers of the FMR1 premutation show altered hippocampal-prefrontal function during memory encoding. *Front Hum Neurosci* 6. [CrossRef](#)
- Zalfa F, Giorgi M, Primerano B, Moro A, Di Penta A, Reis S, Ben Oostra, Bagni C (2003) The fragile X syndrome protein FMRP associates with BC1 RNA and regulates the translation of specific mRNAs at synapses. *Cell* 112:317–327. [Medline](#)
- Zhang Y, Bonnan A, Bony G, Ferezou I, Pietropaolo S, Ginger M, Sans N, Rossier J, Oostra B, LeMasson G, Frick A (2014) Dendritic channelopathies contribute to neocortical and sensory hyperexcitability in Fmr1. *Nat Neurosci* 1–12.